HHS Public Access

Author manuscript

*Top Curr Chem (J)*. Author manuscript; available in PMC 2017 February 01.

Published in final edited form as:

*Top Curr Chem (J)*. 2016 February ; 374(1): . doi:10.1007/s41061-015-0002-2.

# Photo-Triggered Click Chemistry for Biological Applications

**András Herner**[1] and **Qing Lin**[1]

[1]Department of Chemistry, State University of New York at Buffalo, Buffalo, NY 14260, USA

## Abstract

In the last decade and a half, numerous bioorthogonal reactions have been developed with a goal to study biological processes in their native environment, i.e., in living cells and animals. Among them, the photo-triggered reactions offer several unique advantages including operational simplicity with the use of light rather than toxic metal catalysts and ligands, and exceptional spatiotemporal control through the application of an appropriate light source with pre-selected wavelength, light intensity and exposure time. While the photoinduced reactions have been studied extensively in materials research, e.g., on macromolecular surface, the adaptation of these reactions for chemical biology applications is still in its infancy. In this chapter, we review the recent efforts in the discovery and optimization the photo-triggered bioorthogonal reactions, with a focus on those that have shown broad utility in biological systems. We discuss in each cases the chemical and mechanistic background, the kinetics of the reactions and the biological applicability together with the limiting factors.

### Keywords

Bioorthogonal reaction; Photo-triggered reaction; Photoclick; Tetrazole; Nitrile imine; Azirine; Cyclopropenone; *o*-Naphthoquinone methide; *o*-Quinodimethanes; Hetero Diels–Alder reaction

## 1 Introduction

To study biological pathways in living system, it is often necessary to fluorescently label the biomolecules involved in the pathway so that their movement and function can be visualized directly inside a living cell. To this end, click chemistry [1] and many other bioorthogonal reactions have been developed in the last decade and a half, and they all share the following features: (1) the reactants do not interfere with the native biochemical processes inside cells; (2) the reaction rate is comparable to that of a biological process, and (3) the reactants are stable and nontoxic in living cells and animals [2, 3]. Major efforts have been devoted to achieve a faster reaction rate, to improve the physicochemical properties of the reactants such as size, solubility and membrane permeability, and to demonstrate the utilities of these reactions in biological systems. Amongst these reactions, the photo-triggered reactions represent a special class as they generally exhibit a finer control of the reaction initiation and duration, together with greater resolution in space and time. These controls are achieved through the use of an appropriate light source with preselected wavelength, light intensity

✉Qing Lin, qinglin@buffalo.edu.

and exposure time. Because the photo-triggered reactions proceed without the need of metal catalysts and ligands, they are generally less toxic to cells than the metal-catalyzed reactions.

The role of light in the photo-triggered cycloaddition reactions is to generate the reactive species, which then react with their suitable partners present in the biological systems. There are five ways to generate the reactive species through photo irradiations (Scheme 1), including: (a) the formation of radicals with a photo initiator (e.g., from thiols [4, 5]; (b) the rearrangement (e.g., *ortho*-quinodimethanes from *ortho*-methyl phenyl ketones/aldehydes [6], *ortho*-quinone methides from ortho-hydroxibenzyl alcohols [7], azirines [8]; (c) the expulsion of CO (e.g., cyclopropenones [9]); (d) the expulsion of $N_2$ (e.g., tetrazoles); and (e) the removal of photo-cleavable groups (e.g., nitrobenzyls, nitroaryls, coumarins) [10] (Scheme 1). In our review, we will focus on the reactive species that participate in the cycloaddition reactions after their photo-generation.

Depending on their stability, the photo-generated reactive species serving as the cycloaddition partners can be classified into two categories: (a) the reactive species are intrinsically unstable and as a result, they cannot be isolated as discrete compounds using traditional techniques and used as such in the cycloaddition reaction in biological environment (Scheme 2a); and (b) the reactive species are stable but their reactivity are masked in a protected form, which can be unmasked through a burst of light (Scheme 2b). In both cases, the triggering of the downstream cycloaddition reaction requires the photo activation of the precursors, yielding a photo control over the entire process. However, significant differences exist between these two processes: in the former, the photo-generation of the reactive species is irreversible (usually with expulsion of the CO or $N_2$ gas), and the half-life of the unstable reactive species can be tuned through structural modifications; in the latter, the stable intermediate can be reverted back to the unreactive “masked” form through chemical transformations. Furthermore, the long half-life of reactive species in the latter may reduce the spatial resolution as they may diffuse away from the desired subcellular location before encountering its cycloaddition reaction partner in cellular applications.

From the cycloaddition reaction standpoint, the photo-generated reactive species suitable for both 1,3-dipolar cycloaddition reactions and Diels–Alder reactions have been studied in the literature. In this review, we will focus our discussion on four cycloaddition reactions: (1) 1,3-dipolar cycloaddition between alkenes and photo-generated nitrile imines; (2) 1,3-dipolar cycloaddition between alkenes and photo-generated nitrile ylides; (3) photoinduced hetero Diels–Alder reactions; and (4) photoinduced strain promoted azide–alkyne cycloaddition (Scheme 3). It is noteworthy that the majority of photo-generated reactive species serve as either 1,3-dipoles or 1,3-dienes and participate the cycloaddition reactions with appropriately functionalized alkene, presumably due to the lower activation barriers in the concerted processes [11]. Specifically, the following aspects of the reactions will be discussed: (1) the chemical structure, synthesis and substituent effects on reacting partners; (2) the byproducts and possible side products; (3) photophysical parameters including photo-activation wavelength, light intensity, exposure time and quantum yield; (4) the kinetics of the cycloaddition reaction; and (5) the applications in biological systems and potential limiting factors.

# 2 Photoinduced 1,3-Dipolar Cycloaddition Reaction Between Tetrazoles and Alkenes

## 2.1 Theoretical Background and Reaction Mechanism

In the 1960s Huisgen discovered that the photo- or thermo-lysis of 2,5-diphenyl tetrazole (**16**) and treatment of hydrazonyl chlorides (**13**) under basic conditions led to the same pyrazoline cycloadduct (**19**) when methyl crotonate was used as the dipolarophile [12, 13]. The product was a 3:1 isomeric mixture of pyrazolines. After photoirradiation and $N_2$ release, the reactive nitrile imine (**17a**) is generated from tetrazole (**16**) irreversibly. In contrast to other bioorthogonal reactions whereby 1,3-dipoles are generally stable in aqueous medium (e.g., azide and nitrone), nitrile imine reacts with water and therefore needs to be formed in situ. A concerted reaction mechanism was proposed; first the diaryltetrazole (**16**) undergoes facile cycloreversion and generates in situ a nitrile imine dipole (**17a**), which reacts spontaneously with dipolarophiles (e.g., a suitable alkene, **18**) to afford the pyrazoline (**19**) product. The presence of the short-lived nitrile imine was verified by the fragmentation study of the $^{15}N$ enriched tetrazoles at low temperature [14]. A bent nitrile imine geometry was observed directly after photo-irradiating a Zn coordination crystal, and the bent geometry suggested the 1,3-dipolar electronic form (**17a**) (in dashed box in Scheme 4) based on the water-quenching study [15]. For diaryltetrazoles, the photoinduced ring rupture was very efficient in the middle UV region (<290 nm) with a quantum yield of 0.5–0.9 and the substituent effect was not significant [16, 17]. The experimental observation of the major product of the 5-pyrazoline was also supported by theoretical calculations in which the transition state was examined [18]. The cycloaddition is faster in water thanks to the hydrophobic effect [19]. Despite these favorable features, tetrazoles were used mostly in the synthesis of heterocyclic compounds [20, 21] and in polymer and material sciences [22] for a long time.

In addition to the photo-generation, Carell and coworkers showed that the hydrazonyl chloride (**13**) could also serve as a precursor to the reactive nitrile imine (**17a**) in neutral aqueous buffer [23]. Intrigued by these results, Liu and coworkers conducted a mechanistic study of the hydrazonyl chloride-mediated cycloaddition by examining the effects of pH and chloride concentration on the rates of nitrile imine formation and subsequent cycloaddition reactions [24]. They concluded that the cycloaddition reaction is most favorable at basic pH and in the absence of the chloride ion, and that the cycloaddition rate approaches $3.4 \times 10^4$ $M^{-1}$ $s^{-1}$ after factoring in the various equilibria, which makes this cycloaddition one of the fastest click reactions. A plausible mechanism unifying the two nitrile imine generation pathways is shown in Scheme 4, in which water or HCl addition products serve as reservoirs for the unstable nitrile imine prior to the cycloaddition reaction.

## 2.2 Synthesis of Tetrazoles

Two common synthetic routes have been used for the synthesis of tetrazoles (Scheme 5). First, the phenyl sulfonylhydrazones (**23**) react with the freshly prepared diazonium salts (**24**) in pyridine under cooled conditions to produce the desired tetrazole products (**25**) with moderate to good yields [25]. The hydrazones (**23**) can be synthesized easily from the

aliphatic or aromatic aldehydes (**21**) and the diazonium salts from the corresponding amines with $NaNO_2$ under acidic conditions. The second method has been used to prepare the thiophene conjugated tetrazoles (**29**) which exhibit longer photoactivation wavelength [26–28].

### 2.3 Effects of Substrates on Photoactivation Wavelength and Spectral Properties of Pyrazoline

In 2007 we started to study tetrazoles for both synthetic and biological applications. In our first report [29], different solvent systems ranging from nonpolar benzene to $EtOH/H_2O$ (7:3) mixture were investigated along with the study of substituent effect on the phenyl rings (**30**) (Scheme 6a). The photoinduced cycloaddition reaction was found to be very robust with >90 % yields for most substrates along with high solvent tolerance and exclusive regioselectivity with the electron-withdrawing group residing at the $C^5$-position. In addition, it was found that a simple hand-held benchtop UV lamp (UVP, 302 nm, 0.16 AMPS, typically used in the lab for thin layer chromatograph monitoring) was sufficient for driving the reaction to completion, making the reactions very accessible to most chemistry labs.

Since 302-nm UV light may pose considerable phototoxicity to cells [30], for wider use of the tetrazole-based cycloaddition reaction in biological systems it is imperative to shift the photoactivation wavelength to the long-wavelength region. To this end, a series of substituted diaryltetrazoles (**33**) were synthesized (Scheme 6b) [31], and their absorption maxima and absorption coefficients at 365 nm (wavelength of the long-wavelength hand-held UV lamp) were determined in $MeOH/H_2O$ (1:1). It was found that the electron-donating $NH_2$ and $NMe_2$ groups yielded the largest shift in absorption maxima (to 310 and 336 nm, respectively) along with increased absorption coefficients at 365 nm ($0.35 \times 10^4$ and $1.87 \times 10^4$ $M^{-1}$ $cm^{-1}$, respectively).

Additional diaryltetrazole derivatives with potential long wavelength photoactivatability were designed and synthesized based on the ‘scaffold hopping’ strategy (Scheme 7, compounds **36–40**) [32]. Extension of the aromatic conjugation system provided a bathochromic shift of the photoactivation wavelength. These tetrazoles underwent efficient ring rupture upon 365 nm photoirradiation and generated the brightly fluorescent pyrazoline products after the cycloaddition reaction, which could be useful for visualization of the alkene-tagged proteins in living cells. Separately, appending oligothiophenes to the tetrazole core provided further shift in absorption maxima close to 405 nm, a wavelength for a commonly used laser source on microscopes (Scheme 7, compounds **41–45**) [28]. The quantum yield for 405 nm laser-induced ring rupture was determined to be 0.16, significantly higher than the reported 365-nm photoactivatable tetrazoles ($\Phi$ = 0.006–0.04) [31]. A water-soluble derivative of **43**, compound **55**, exhibited second order rate constant, $k_2$, of 1299 ± 110 $M^{-1}$ $s^{-1}$ in the cycloaddition reaction with mono-methyl fumarate amide in MeCN/PBS (1:1). In addition, compound **55** was shown to selectively image the microtubules in CHO cells in a spatiotemporally controlled manner when the cells were pre-treated a fumarate modified docetaxel **56** (Fig. 1). To fine-tune the emission wavelength of the resulting pyrazoline adducts, additional dithiophene-containing tetrazole analogs were prepared (Scheme 7, compounds **46–54**) [33]. These compounds showed fast kinetics in the

reaction with dimethyl fumarate ($k_2$ up to 3960 $M^{-1}$ $s^{-1}$ in 1:1 PBS/MeCN) upon 405-nm photoirradiation, and most importantly, provided the red fluorescent pyrazoline adducts (emission maxima in the range of 575–644 nm in 1:1 PBS/MeCN) in excellent yields.

To reduce light scattering and improve three dimensional localization of excitation, the two-photon excitation (2PE) of tetrazoles was demonstrated with the naphthalene-based derivatives [34]. By taking advantage of the known 2PE of naphthalene [35], various naphthalene-based tetrazole derivatives were synthesized and tested (**57–59**) (Fig. 2). A femtosecond 700 nm near infrared (NIR) pulsed laser source was used for initiating the photoclick chemistry in this study. The two-photon absorption cross section ($\delta_{aT}$) of tetrazole **59** was determined to be 12 GM (=$10^{-50}$ $cm^4$ s/photon) and the cycloaddition cross section was 3.8 GM, comparable to the uncaging efficiency of the commonly used two-photon protecting group, 6-bromo-7-hydroxycoumarin-4-ylmethyl acetate ($\delta_{ur}$ = 0.95 GM), under similar conditions [36]. Under the 2PE conditions, tetrazole **59** was used successfully in the labeling of the acrylamide-tagged GFP in PBS in vitro as well as the imaging of the microtubules in a spatiotemporally controlled manner in live CHO cells treated with the fumarate-modified docetaxel **56** (Fig. 2).

## 2.4 Site-Specific Labeling of Proteins Via the Photoinduced Tetrazole–Alkene Cycloaddition

One of the important applications of bioorthogonal reactions is labeling of proteins carrying amino acid side chains with unique chemical reactivity in their native environment [37]. This is usually accomplished in two steps: (1) a bioorthogonal reporter is introduced into the protein of interest; and (2) a biophysical probe with the cognate chemical reactivity reacts with the pre-tagged protein selectively. For the photoclick chemistry, the introduction of an alkene or a tetrazole can be achieved using either in vitro modification of the native protein side chains (e.g., Cys and Lys) or unnatural amino acids (UAAs) carrying the suitable functionality in vivo (Scheme 8) [38]. In general, the genetic approach in encoding of UAAs has overcome many disadvantages associated with the native residue-based chemistry, e.g., low selectivity, and as a result, has gained increasing popularity in protein science whenever specific protein modifications are needed, both in vitro and in vivo.

In the very first application of the tetrazole-based cycloaddition chemistry to proteins [39], a carboxylic acid functionalized tetrazole was coupled to a tripeptide (RGG) and the kinetics of the cycloaddition reaction between the tetrazole-modified peptide and acrylamide was investigated under the 302-nm photoirradiation condition. The photolysis of the tetrazole-modified peptide to its corresponding nitrile imine was extremely rapid with a first-order rate constant to be 0.14 $s^{-1}$; the subsequent cycloaddition with acrylamide proceeded with a second-order rate constant, $k_2$, of 11.0 $M^{-1}$ $s^{-1}$. In the next step, the surface Lys residues of lysozyme were modified with a water-soluble tetrazole succinimide (**60**), and the resulting tetrazole-modified lysozyme was irradiated with 302 nm light for 2 min in the presence of acrylamide (Scheme 8a). The LC–MS analysis indicated that the conversion of the tetrazole-modified lysozyme to the pyrazoline adduct was very specific with an estimated yield around 90 %. We also prepared a tetrazole-containing enhanced green fluorescent protein, EGFP-Tet, using the intein-based chemical ligation strategy (Scheme 8a). The photo-

triggered cycloaddition reaction between EGFP-Tet and *N*-hexadecylmethacrylamide proceeded in bacterial lysate with ~52 % conversion based on LC–MS analysis. The application of the tetrazole-modified EGFP was also used to probe the effect of lipidation on protein localization in live cells without the use of lipidation enzymes [40].

The tetrazole-based cycloaddition chemistry was subsequently applied to protein labeling in bacteria cells via a genetically encoded *O*-allyl-tyrosine (***O*-allyl-Tyr**, Scheme 8c) [41]. In this study, the reactions between tetrazole derivatives and allyl phenyl ether were first investigated. The formation of nitrile imine was found to be fast (<2 min) but the cycloaddition steps was slow ($k_2$ = 0.00202 $M^{-1}$ $s^{-1}$ with allyl phenyl ether in 1:1 PBS/MeCN; 75-fold slower than acrylamide). In-gel fluorescence-based screen identified 4-(methoxycarbonyl)phenyl substituted tetrazole in the $C_5$-position from a panel of tetrazole compounds as a suitable reagent for selective labeling of *O*-allyl-tyrosine-encoded Z-domain protein, which was then used to image the same protein in *E. coli* cells. Since the reaction rate is inversely related to the energy gap between $HOMO_{dipole}$ and $LUMO_{dipolarophile}$ in the nitrile imine–alkene cycloaddition [18], it was envisioned that raising the HOMO energy of the nitrile imine should lead to reaction acceleration. Thus, a series of substituted diaryltetrazoles were synthesized and their reaction rates toward 4-penten-1-ol were measured [42]. It was found that the electron-donating substituents on the $N^2$-phenyl ring such as $–NH_2$ and –OMe groups significantly raise the HOMO energies of the photo-generated nitrile imine dipoles, with second-order rate constants reaching as high as 0.79 $M^{-1}$ $s^{-1}$ in 1:1 PBS/MeCN. Furthermore, a methoxy-substituted diphenyltetrazole was shown to label the *O*-allyl-tyrosine-encoded Z-domain proteins in *E. coli* in <1 min.

To overcome slow reaction kinetics observed with the genetically encoded system, two complementary efforts were untaken. One approach was to incorporate the tetrazole moiety into the amino acid side chain and evolve orthogonal aminoacyl-tRNA synthetase/tRNA pairs to charge the resulting tetrazole amino acids into proteins site-specifically. To this end, we synthesized a series of tetrazole modified unnatural amino acids (Scheme 8b), and tested their reactivity in the photo-triggered cycloaddition reaction with methyl methacrylate in PBS/MeCN (1:1) [43]. While four out of six tetrazole amino acids gave excellent reaction yields, only *p*-tetrazole-phenylalanine (***p*-Tpa**) was incorporated into myoglobin site-specifically using an evolved synthetase via the amber codon suppression [44]. A drawback of this genetically encodable tetrazole amino acid is that a 254-nm UV light is needed for triggering the reaction because of the shortened **π**-conjugation system. In addition, the cycloaddition reaction with dimethyl fumarate proceeded rather sluggishly, with a measured $k_2$ value of 0.082 ± 0.011 $M^{-1}$ $s^{-1}$ in 1:1 PBS/MeCN.

The second approach focused on the genetic encoding of the reactive alkene-containing amino acids, which are in general smaller than the tetrazole amino acids and thus easier to derive the specific orthogonal aminoacyl-tRNA synthetase/tRNA pairs (Scheme 8c). To increase alkene reactivity in the photoclick chemistry without unwanted side reactions such as Michael addition, ring strain has been successfully exploited. In 2010, we showed that norbornene served as an excellent substrate in the photo-triggered cycloaddition reaction with the macrocyclic tetrazoles [45]. Later, Carell and co-workers showed that a norbornene-modified Lys (**68**) can be genetically encoded into $His_6$-tagged human polymerase **κ**, and

that efficient labeling of polymerase κ can be accomplished with the nitrile imines generated from either the hydrazonyl chloride precursor or the corresponding tetrazole [23]. The utility of the norbornene modified amino acids was also demonstrated in the tetrazine ligation in eukaryotic cells by other research groups [46–48]. Smaller strained alkenes such as cyclopropene have also been developed for the photoclick chemistry. Cyclopropene has a ring strain of 54.1 kcal $mol^{-1}$ [49] versus 21.6 kcal $mol^{-1}$ for norbornene [50]; after cycloaddition, the cyclopropane product has a decreased strain of 28.7 kcal $mol^{-1}$ [51]. Based on these considerations, we synthesized a cyclopropene modified Lys, **CpK**, and showed that **CpK** can be site-specifically incorporated into proteins using the amber codon suppression strategy [52]. Fast cycloaddition kinetics was observed with the 3,3-disubstituated cyclopropene in 1:1 PBS/MeCN; the second-order rate constant was determined to be 58 ± 16 $M^{-1}$ $s^{-1}$ (for comparison: $k_2$ = 46 ± 9 $M^{-1}$ $s^{-1}$ for acryl amide, 32 ± 12 $M^{-1}$ $s^{-1}$ for norbornene, and 0.95 $M^{-1}$ $s^{-1}$ for allyl phenyl ether). Importantly, **CpK** was shown to direct site-specific modification of green fluorescent protein inside HEK293T cells via the tetrazole-based photoclick chemistry. Notably, the cyclopropene moiety has also been used as a reaction partner in tetrazine ligation [53, 54], with its reactivity preference between the tetrazine and tetrazole chemistries depending on the substitution pattern [55]. Realizing the cyclopropene reactivity can be further increased by reducing the steric hindrance at position 3, we fused a cyclobutane ring with the cyclopropene to generate spiro[2.3]hex-1-ene (**Sph**) [56]. Sph reacted with methoxy-diphenyltetrazole in $CD_3CN$ 17-times faster than the 3,3-disubstitued cyclopropene. A spiro[2.3]hex-1-ene modified lysine (**SphK**) was synthesized and shown to be successfully incorporated into the superfolder GFP (sfGFP) using the wild-type PylRS/tRNA pair. To our delight, the **SphK**-encoded sfGFP displayed a fast reaction kinetics with a water-soluble tetrazole in phosphate buffer in the photo-triggered cycloaddition reaction with a measured $k_2$ value of 1.0 × $10^4$ $M^{-1}$ $s^{-1}$, comparable to the typical tetrazine-*trans*-cyclooctene cycloaddition reaction ($k_2$ = 2.2 × $10^4$ $M^{-1}$ $s^{-1}$) [57].

On the other hand, Liu and co-workers demonstrated the accelerated photoclick chemistry with proteins using the electron-deficient acrylamide modified lysine (**AcrK**) [58]. The basis for faster kinetics with acrylamide is its lower LUMO energy compared to allyl phenyl ether. The **AcrK**-encoded sfGFP was successfully labeled with the hydrazonyl chloride precursor. The utility of AcrK was further demonstrated with fluorescent labeling of an overexpressed membrane protein OmpX in *E. coli.* Independently, Wang and co-workers evolved an orthogonal tRNA/aminoacyl-tRNA synthetase pair that allowed selective incorporation of **AcrK** into bacterial tubulin-like cytoskeleton protein FtsZ [59]. The utility of **AcrK** in the tetrazole-based photoclick chemistry was demonstrated with the purified proteins in vitro as well as in *E. coli* and mammalian cells. Additionally, **AcrK** was incorporated into GFP-TAG-mCherry-HA protein in *Arabidopsis thaliana*, a commonly used plant model.

The recent development of super-resolution microscopic techniques (PALM [60] and STORM [61]) has demanded new photoactivatable fluorophores with high turn-on efficiency and excellent biocompatibility. Realizing that the pyrazoline adducts formed from the photo-triggered cycloaddition reaction are fluorescent, we envisioned that a new type of fluorescent turn-on probes can be desired by combining the tetrazole and alkene groups on

the same molecule [62]. The resulting alkene-modified tetrazoles (**69**) can be efficiently activated using a mild UV light source (302 or 365 nm), and the pyrazoline products (**70**) can be readily monitored under fluorescence microscope. We demonstrated this intramolecular cycloaddition reaction approach to turn-on probe design by imaging the microtubules in intact CHO cells treated with the alkene–tetrazole modified paclitaxel derivatives (**69**, Scheme 9). Similarly, the tetrazole-based intramolecular photoclick chemistry was also applied to synthesize the side chain-crosslinked peptides [63]. Briefly, the tetrazole and acrylamide modified lysine or ornithine were incorporated into a model $3_{10}$-helical peptide [64, 65]. After photoirradiation, the pyrazoline-cross-linked peptides were generated in high yields. This tetrazole-based photo-crosslinking strategy was later successfully applied to the synthesis of cell-permeable peptide dual inhibitors of the p53-Mdm2/Mdmx interactions [66].

The development of smart hydrogels as extracellular matrices has shown growing importance in cell culture [67]. By taking advantage of the spatiotemporal control of the photo-responsible compounds, Zhong and co-workers used the photo-triggered tetrazole–methacrylate cycloaddition reaction to generate the hydrogels (Fig. 3a) [68]. This photo-triggered gelation approach offered a number of advantages, including tunable gelation by varying exposure time, high specificity and conversion, and avoidance of protein denaturation. Separately, Zhang and co-workers applied the intramolecular tetrazole-based photoclick chemistry to regulate the self-assembly of the hydrogels (Fig. 3b) [69]. Irradiation of the hydrogels induced degradation of the supramolecular matrix, which led to the release of encapsulated biological materials such as proteins and cells. For example, the photo-triggered release control of the encapsulated horse serum was shown, which induced the differentiation of C2C12 cells [70] on top of the hydrogels.

## 3 1,3-Dipolar Cycloaddition Reaction Between Azirines and Alkenes

Photo-triggered ring opening of 2*H*-azirines is a well-known reaction to produce pyrrolines [8, 71]. Padwa and co-workers showed that photoirradiation of azirines with a mercury arc lamp (450 W) equipped with Vycor filter generated the reactive nitrile ylide intermediate (**72**), which can be stabilized by the phenyl substituents. The nitrile ylide (**72**) then reacts with the electron-deficient olefins (**73**) such as acrylate and acrylonitrile in a cycloaddition reaction to form $\Delta^1$-pyrrolines (**74**) (Scheme 10) [8]. Steenken and co-workers studied reaction kinetics of azirines with dipolarophiles as well as nucleophiles such as alcohols [72]. They showed that the reaction rate depends on the azirine substituents, the nucleophilicity of the reactant and the acidity of the alcohol.

In 2010, we reported the first use of photo-triggered azirines-mediated cycloaddition reaction for selective protein modification in biological buffer (Scheme 11) [73]. A series of azirines were synthesized and their reactions with 2-methylmethacrylate and dimethyl fumarate in EtOH/$H_2O$ (1:1) were investigated. The photo-generated nitrile ylide intermediate was not detected in the HPLC analysis, suggesting that the rate-determining step is likely the azirine ring opening with a measured first-order rate constant of 0.0379 $s^{-1}$. Furthermore, an azirine-modified lysozyme was selectively functionalized by a water-

soluble PEGylated fumarate (**78**) after 2 min 302-nm photoirradiation. The major limitation of this reaction is the need of highly electron-deficient dipolarophiles such as fumarate.

Very recently, Blinco and Barner-Kowollik have successfully shifted the photoactivation wavelength into the visible region (>390 nm) [74]. By replacing the phenyl group with the pyrene group on the azirine ring, they showed that the photo-triggered cycloaddition proceeded in <1 min under ambient conditions with the electron-deficient alkenes such as fumarates, maleimide, acrylates, and activated acetylenes. Reactions were initiated using a photoreactor equipped with an LED light (410–420 nm, 3 W). The utility of this modified reaction was demonstrated through efficient conjugation of PEG chains to the pyrene fluorophore.

## 4 Photoinduced Hetero Diels–Alder Reactions

Diels–Alder (DA) reaction is one of the most useful chemical transformations. This reaction typically proceeds slowly in the absence of a catalyst, but can be accelerated with the use of Lewis acids [75]. It is characterized by high yield under various conditions, has less sensitivity against solvents, and does not produce byproducts. It is characterized by high yield under various conditions, insensitive toward solvent polarity, and little byproducts. Indeed, the tetrazine/*trans*-cyclooctene based inverse electron-demand DA reaction has become the most popular bioorthogonal reaction in the literature because of its fast reaction kinetics [76]—second-order rate constant as high as $2.8 \times 10^6\ M^{-1}\ s^{-1}$ has been reported [77]. So far, two photo-triggered hetero-dienes have been exploited in the DA reactions for biological use, namely, *o*-quinone methides and hydroxy-*o*-quinodimethanes.

### 4.1 Naphthoquinone Methide

In 2011, Popik and co-workers reported photochemical dehydration of 3-hydroxy-2-naphthalenemethanol (*o*-naphthoquinone precursor, NQMP, **79**) derivatives to *o*-naphthoquinone methides (*o*NQMs, **80**) [78, 79]. The in situ generated reactive intermediate *o*NQM underwent facile cycloaddition with vinyl ethers (**81**) to form photostable benzochromans (**82**) (Scheme 12). NQMP (**79**) has two major absorption bands at 275 nm (log ε = 4.06) and 324 nm (log ε = 3.70); thus it can be photoactivated with either low pressure mercury lamp (254 nm) or fluorescent tubes (300 and 350 nm). The quantum yield of the photoactivation was very high ($\Phi_{300} = 0.17 \pm 0.02$ for **79**). The in situ generated *o*NQMs was quenched mostly by water with a high reaction rate ($k_w = 145\ s^{-1}$ or $2.61\ M^{-1}\ s^{-1}$), which regenerates the starting material. When vinyl ethers was present, *o*NQMs underwent rapid cycloaddition reaction with a second order rate constant in the range of $4–6 \times 10^4\ M^{-1}\ s^{-1}$ in PB/MeCN (1:1). For photoirradiation, samples were exposed to 4-W 300-nm fluorescent tubes for 3 min (~15 % conversion) or 20 min (>99 % conversion). Notably, 350-nm fluorescent tubes also worked with longer exposure time, presumably due to the lower absorption at this wavelength.

When other alkenes such as methyl acrylate, dimethyl maleate, 2,5-dihydrofurans and methyl cyclohexene were present in a competition reaction, only alkyl vinyl ethers produced the desired benzochroman cycloadducts (**84**) (Scheme 13). Mechanistic studies revealed that

the key issue is the competition with hydration. Apparently, the cycloaddition reactions with the non-polarized electron-deficient alkenes could not compete with the water-quenching.

Since acetals are susceptible to hydrolysis, the adjustment of solution pH offers a control over the product stability; at neutral or basic pH, no hydrolysis would occur. The enamines (**86**) are another class of electron-rich polarized alkenes which could undergo facile cycloaddition reaction with *o*NQMs (**80**), but the primary cycloadducts (**88**) rapidly hydrolyze in aqueous medium to produce 2-hydroxybenzochromanes (**90**). Nevertheless, this method is suitable for the introduction of functional groups at position 3 of the benzochromane (**90**) (Scheme 14).

Reactive *o*NQMs (**80**) can also be efficiently captured by strong nucleophiles such as thiols presented in millimolar concentrations in biological systems. They observed thiol addition ($k_2 = 2.2 \times 10^5\ M^{-1}\ s^{-1}$ with thioethanolamine; 5-times faster than the DA reaction with ethyl vinyl ether). However, the adduct was photochemically labile; upon longer irradiation time (30 min instead of 20 min) it was converted back to NQMP **79**) (Scheme 14). The feature that oNQMs react faster with thiols (in reversible way) but slower than vinyl ethers (in irreversible way) was exploited in the controlled release of thiol functionalized compounds *o*NQMs (Scheme 15) [80]. First, with a short irradiation (2–5 min, 300 or 350 nm) the thiol adduct (**92**) was formed, which was later released quantitatively with 2–5 min (350 nm) irradiation in the presence of ethyl vinyl ether. Selective and reversible functionalization of proteins was achieved through Cys modification. Reversibility was also shown with photoinitiated capture and hydrolytic cleavage (Scheme 15) [81].

Lei and coworkers modified this structure to allow a reaction with vinyl thioethers (VT) to form a stable covalent bond [82]. The biological utility was demonstrated by labeling a VT-modified BSA and imaging a VT-modified taxol in live HeLa cells. Introducing a N into the aromatic system eliminate the need for irradiation, therefore losing the advantage provided by photoinitiation.

### 4.2 *o*-Quinodimethane

Photoenolization of *ortho*-methyl phenyl ketones and aldehydes (**96**) has been used in organic chemistry for a long time [6, 83, 84]. The first application of this reaction in polymer science was made by Barner-Kowollik et al. [85]. Irradiation leads to formation of biradicals (**99**) that rearrange to highly reactive diene (hydroxy-*o*-quinodimethane or “photoenol”, **100**). This intermediate **100** reacts with electron-deficient dienophiles (**101**) such as maleimide via Diels–Alder reaction (Scheme 16). The driving force is the restored aromaticity. In their study, two polymers were coupled through maleimide and *o*-methyl phenyl ketone functional groups irradiated with compact fluorescence lamp (36 W, $\lambda_{max}$ = 320 nm) in toluene for 20–100 min at ambient temperature. Triblockpolymers were synthesized using the same strategy [86].

Later, the same group modified the structure of *o*-methyl phenyl ketone to 2-formyl-3-methylphenoxy (FMP, **103**) and reached higher reactivity towards the alkene dienophiles (Scheme 17) [87]. They assumed that after photoexcitation the hydrogen bond formation stabilizes the reactive intermediate (**104**) by increasing both its lifetime and ratio of formed

*Z* isomer, which has higher reactivity towards dienophiles relative to the *E* isomer [88]. The less electron-deficient acrylates, which cannot react with the original hydroxy-*o*-quinodimethane, can now be used with FMP [89]. Full conversion with maleimide was reached in <15 min in acetonitrile and dichloromethane. While the reaction is water compatible, long time is needed when the reactions are performed in polar solvents such as water and DMF in order to achieve full conversion. For biological applications, a preliminary study was carried out with the maleimide-oligopeptide conjugate (**105**). The product was formed in quantitative yield from the peptide and the FMP (**103**) in PBS/MeCN (1:3) under 320 nm irradiation. Full conversion was reached after 2 h photoirradiation. Patterning of silicon surfaces with oligopeptides (GRGSGR) was also demonstrated.

## 5 Strain-Promoted Azide–Alkyne Cycloaddition

Copper-catalyzed azide–alkyne cycloaddition (CuAAC) is one of the most powerful click reactions. The only disadvantage is that the copper is toxic to certain cells [90]. Despite efforts to make the copper complexes more biocompatible [91, 92], the breakthrough was achieved by the Bertozzi group [93] through harnessing the ring strain present in cyclooctyne to accelerate the reaction. A variety of cyclooctynes and one cycloheptyne have subsequently been reported [94, 95].

Based on the earlier studies of using cyclopropenone (CP) [9, 96] as a photo-protected precursor of alkyne, Popik and co-workers combined this feature with the click chemistry (**109–110**) (Scheme 18) [97]. The CP is thermally stable in aqueous solution and reacts with azides exclusively after photoirradiation. High quantum yield was measured for the photo-decarbonylation step ($\Phi_{355}$ = 0.33) and the corresponding alkyne (**111–112**) was obtained in quantitative yield. The cycloaddition rate was determined to be 1.6–7.6 × $10^{-2}$ $M^{-1}$ $s^{-1}$ in MeOH. For biological applications, Jurkat cells were cultured in the presence of peracetylated *N*-azidoacetyl mannosamine ($Ac_4$ManNAz). After incubation with a biotin-modified CP (**113**) and 1 min irradiation at 350 nm, the labeling efficiency was evaluated with avidin-fluorescein isothiocyanate (FITC). The labeling efficiencies were comparable between the in situ formed cyclooctyne and the unprotected one. Without photoirradiation, the background labeling was negligible. The temporal control could not be demonstrated because of 30-min delay between the irradiation and fluorescence acquisition. One disadvantage of CP reagent is that it is prone to nucleophilic attack by endogenous thiols [9].

## 6 General Conclusions

For a long time, photo-triggered click chemistry has been used mostly in material sciences. With the recent design and synthesis of some new reagents, these reactions have begun to be employed in bioorthogonal chemistry based studies. The advantages of light-induced spatiotemporal control has been harnessed for selective labeling of the biomolecules in living system. Table 1 summarizes the optimized parameters achieved so far with the best reactant pairs for each of these photo-triggered cycloaddition reactions. In conjunction of the recent rapid development of synthetic biology in which the unique chemical groups are added to cell's basic building blocks, we anticipate the photo-triggered bioorthogonal

reactions will offer an unprecedented spatiotemporally controlled chemical tool to dissect complex biological processes in their native environments.

## Acknowledgments

Work on the tetrazole-based photoclick chemistry in QL lab was supported by the National Institutes of Health (GM 085092). AH thanks the Rosztoczy Foundation (to A.H.) for a scholarship.

## Abbreviations

| | |
|---|---|
| **2PE** | Two-photon excitation |
| **CuAAC** | Cu-catalyzed azide–alkyne cycloaddition |
| **DA** | Diels–Alder |
| **ε** | Absorption coefficient |
| **Φ** | Quantum yield |
| **HOMO** | Highest occupied molecular orbital |
| **λ** | Wavelength |
| **LUMO** | Lowest unoccupied molecular orbital |
| **PB** | Phosphate buffer |
| **PBS** | Phosphate buffered saline |
| **PG** | Protecting group |
| **SPAAC** | Strain-promoted azide–alkyne cycloaddition |
| **UAA** | Unnatural amino acid |
| **UV** | Ultraviolet |

## References

1. Kolb HC, Finn MG, Sharpless KB. Angew Chem Int Ed. 2001; 40:2004.
2. Saxon E, Bertozzi CR. Science. 2000; 287:2007. [PubMed: 10720325]
3. Prescher JA, Bertozzi CR. Nat Chem Biol. 2005; 1:13. [PubMed: 16407987]
4. Lowe AB. Polym Chem. 2014; 5:4820.
5. Lowe AB. Polymer. 2014; 55:5517.
6. Sammes PG. Tetrahedron. 1976; 32:405.
7. Diao L, Yang C, Wan P. J Am Chem Soc. 1995; 117:5369.
8. Padwa A. Acc Chem Res. 1976; 9:371.
9. Poloukhtine A, Popik VV. J Org Chem. 2003; 68:7833. [PubMed: 14510563]
10. Mayer G, Heckel A. Angew Chem Int Ed. 2006; 45:4900.
11. Su MD, Liao HY, Chung WS, Chu SY. J Org Chem. 1999; 64:6710. [PubMed: 11674676]
12. Huisgen R, Seidel M, Wallbillich G, Knupfer H. Tetrahedron. 1962; 17:3.
13. Clovis JS, Eckell A, Huisgen R, Sustmann R. Chem Ber. 1967; 100:60.

14. Toubro NH, Holm A. J Am Chem Soc. 1980; 102:2093.
15. Zheng SL, Wang Y, Yu Z, Lin Q, Coppens P. J Am Chem Soc. 2009; 131:18036. [PubMed: 19928921]
16. Weinberg P, Csongar C, Grummt UW. J Photochem Photobiol A. 1989; 50:11.
17. Lohse V, Leihkauf P, Csongar C, Tomaschewski G. J Prakt Chem. 1988; 330:406.
18. Houk KN, Sims J, Watts CR, Luskus LJ. J Am Chem Soc. 1973; 95:7301.
19. Molteni G, Orlandi M, Broggini G. J Chem Soc Perk Trans. 2000; 1:3742.
20. Padwa A, Nahm S, Sato E. J Org Chem. 1978; 43:1664.
21. Meier H, Heimgartner H. Helv Chim Acta. 1985; 68:1283.
22. Darkow R, Yoshikawa M, Kitao T, Tomaschewski G, Schellenberg J. J Polym Sci A Polym Chem. 1994; 32:1657.
23. Kaya E, Vrabel M, Deiml C, Prill S, Fluxa VS, Carell T. Angew Chem Int Ed. 2012; 51:4466.
24. Wang XS, Lee YJ, Liu WR. Chem Commun. 2014; 50:3176.
25. Ito S, Tanaka Y, Kakehi A, Kondo K. Bull Chem Soc Jpn. 1976; 49:1920.
26. Koguro K, Oga T, Mitsui S, Orita R. Synthesis. 1998; 6:910.
27. Lenda F, Guenoun F, Tazi B, Larbi NB, Allouchi H, Martinez J, Lamaty F. Eur J Org Chem. 2005; 326
28. An P, Yu Z, Lin Q. Chem Commun. 2013; 49:9920.
29. Wang Y, Rivera Vera CI, Lin Q. Org Lett. 2007; 9:4155. [PubMed: 17867694]
30. Wells RL, Han A. Int J Radiat Biol. 1985; 47:17.
31. Wang Y, Hu WJ, Song W, Lim RKV, Lin Q. Org Lett. 2008; 10:3725. [PubMed: 18671406]
32. Yu Z, Ho LY, Wang Z, Lin Q. Bioorg Med Chem Lett. 2011; 21:5033. [PubMed: 21570845]
33. An P, Yu Z, Lin Q. Org Lett. 2013; 15:5496. [PubMed: 24111736]
34. Yu Z, Ohulchanskyy TY, An P, Prasad PN, Lin Q. J Am Chem Soc. 2013; 135:16766. [PubMed: 24168622]
35. McClure DS. J Chem Phys. 1954; 22:1668.
36. Furuta T, Wang SS, Dantzker JL, Dore TM, Bybee WJ, Callaway EM, Denk W, Tsien RY. Proc Natl Acad Sci USA. 1999; 96:1193. [PubMed: 9990000]
37. Lang K, Chin JW. ACS Chem Biol. 2014; 9:16. [PubMed: 24432752]
38. Liu CC, Schultz PG. Annu Rev Biochem. 2010; 79:413. [PubMed: 20307192]
39. Song W, Wang Y, Qu J, Madden MM, Lin Q. Angew Chem Int Ed. 2008; 47:2832.
40. Song W, Yu Z, Madden MM, Lin Q. Mol BioSyst. 2010; 6:1576. [PubMed: 20436975]
41. Song W, Wang Y, Qu J, Lin Q. J Am Chem Soc. 2008; 130:9654. [PubMed: 18593155]
42. Wang Y, Song W, Hu WJ, Lin Q. Angew Chem Int Ed. 2009; 48:5330.
43. Wang Y, Lin Q. Org Lett. 2009; 11:3570. [PubMed: 19637915]
44. Wang J, Zhang W, Song W, Wang Y, Yu Z, Li J, Wu M, Wang L, Zang J, Lin Q. J Am Chem Soc. 2010; 132:14812. [PubMed: 20919707]
45. Yu Z, Lim RKV, Lin Q. Chem Eur J. 2010; 16:13325. [PubMed: 21031376]
46. Lang K, Davis L, Torres-Kolbus J, Chou C, Deiters A, Chin JW. Nat Chem. 2012; 4:298. [PubMed: 22437715]
47. Plass T, Milles S, Koehler C, Szymański J, Mueller R, Wießler M, Schultz C, Lemke EA. Angew Chem Int Ed. 2012; 124:4166.
48. Bianco A, Townsley FM, Greiss S, Lang K, Chin JW. Nat Chem Biol. 2012; 8:748. [PubMed: 22864544]
49. Bach RD, Dmitrenko O. J Am Chem Soc. 2004; 126:4444. [PubMed: 15053635]
50. Schleyer PVR, William JE, Blanchard KR. J Am Chem Soc. 1970; 92:2377.
51. Gordon MS. J Am Chem Soc. 1980; 102:7419.
52. Yu Z, Pan Y, Wang Z, Wang J, Lin Q. Angew Chem Int Ed. 2012; 51:10600.
53. Patterson DM, Nazarova LA, Xie B, Kamber DN, Prescher JA. J Am Chem Soc. 2012; 134:18638. [PubMed: 23072583]

54. Yang J, Seckute J, Cole CM, Devaraj NK. Angew Chem Int Ed. 2012; 51:7476.
55. Kamber DN, Nazarova LA, Liang Y, Lopez SA, Patterson DM, Shih HW, Houk KN, Prescher JA. J Am Chem Soc. 2013; 135:13680. [PubMed: 24000889]
56. Yu Z, Lin Q. J Am Chem Soc. 2014; 136:4153. [PubMed: 24592808]
57. Taylor MT, Blackman ML, Dmitrenko O, Fox M. J Am Chem Soc. 2011; 133:9646. [PubMed: 21599005]
58. Lee Y-J, Wu B, Raymond JE, Zeng Y, Fang X, Wooley KL, Liu WR. ACS Chem Biol. 2013; 8:1664. [PubMed: 23735044]
59. Li F, Zhang H, Sun Y, Pan Y, Zhou J, Wang J. Angew Chem Int Ed. 2013; 52:9700.
60. Betzig E, Patterson GH, Sougrat R, Lindwasser OW, Olenych S, Bonifacino JS, Davidson MW, Lippincott-Schwartz J, Hess HF. Science. 2006; 313:1642. [PubMed: 16902090]
61. Rust MJ, Bates M, Zhuang X. Nat Methods. 2006; 3:793. [PubMed: 16896339]
62. Yu Z, Ho LY, Lin Q. J Am Chem Soc. 2011; 133:11912. [PubMed: 21736329]
63. Madden MM, Rivera Vera CI, Song W, Lin Q. Chem Commun. 2009; 5588
64. Karle IL, Flippen-Anderson JL, Uma K, Balaram P. Proteins. 1990; 7:62. [PubMed: 2330369]
65. Karle IL, Flippen-Anderson JL, Uma K, Balaram P. Biopolymers. 1993; 33:827. [PubMed: 8343578]
66. Madden MM, Muppidi A, Li Z, Li X, Chen J, Lin Q. Bioorg Med Chem Lett. 2011; 21:1472. [PubMed: 21277201]
67. Alge DL, Anseth KS. Nat Mater. 2013; 12:950. [PubMed: 24150411]
68. Fan Y, Deng C, Cheng R, Meng F, Zhong Z. Biomacromolecules. 2013; 14:2814. [PubMed: 23819863]
69. He M, Li J, Tan S, Wang R, Zhang Y. J Am Chem Soc. 2013; 135:18718. [PubMed: 24106809]
70. Simone C, Forcales SV, Hill DA, Imbalzano AN, Latella L, Puri PL. Nat Genet. 2004; 36:738. [PubMed: 15208625]
71. Padwa A, Smolanoff J. J Am Chem Soc. 1971; 93:548.
72. Albrecht E, Mattay J, Steenken S. J Am Chem Soc. 1997; 119:11605.
73. Lim RKV, Lin Q. Chem Commun. 2010; 46:7993.
74. Mueller JO, Schmidt FG, Blinco JP, Barner-Kowollik C. Angew Chem Int Ed. 2015; 54:10284.
75. Carey, FA.; Sundberg, RJ. Advanced organic chemistry: part b: reactions and synthesis. 5th. New York: Springer; 2007. p. 481-487.E-ISBN 978-0-387-44899-2 (part B)
76. Liu F, Paton RS, Kim S, Liang Y, Houk KN. J Am Chem Soc. 2013; 135:15642. [PubMed: 24044412]
77. Rossin R, van den Bosch SM, ten Hoeve W, Carvelli M, Versteegen RM, Lub J, Robillard MS. Bioconj Chem. 2013; 24:1210.
78. Arumugam S, Popik VV. J Am Chem Soc. 2011; 133:15730. [PubMed: 21861517]
79. Arumugam S, Orski SV, Locklin J, Popik VV. J Am Chem Soc. 2012; 134:179. [PubMed: 22191601]
80. Arumugam S, Guo J, Mbua NE, Friscourt F, Lin N, Nekongo E, Boons GJ, Popik VV. Chem Sci. 2014; 5:1591. [PubMed: 24765521]
81. Arumugam S, Popik VV. J Org Chem. 2014; 79:2702. [PubMed: 24548078]
82. Li Q, Dong T, Liu X, Lei X. J Am Chem Soc. 2013; 135:4996. [PubMed: 23521211]
83. Charlton JL, Alauddin MM. Tetrahedron. 1987; 43:2873.
84. Segura JL, Martin N. Chem Rev. 1999; 99:3199. [PubMed: 11749515]
85. Gruendling T, Oehlenschlaeger KK, Frick E, Glassner M, Schmid C, Barner-Kowollik C. Macromol Rapid Commun. 2011; 32:807. [PubMed: 21469243]
86. Glassner M, Oehlenschlaeger KK, Gruendling T, Barner-Kowollik C. Macromolecules. 2011; 44:4681.
87. Pauloehrl T, Delaittre G, Winkler V, Welle A, Bruns M, Boerner HG, Greiner AM, Bastmeyer M, Barner-Kowollik C. Angew Chem Int Ed. 2012; 51:1071.
88. Mellows SM, Sammes PG. J Chem Soc Chem Comm. 1971; 21

89. Winkler M, Mueller JO, Oehlenschlaeger KK, de Espinosa LM, Meier MAR, Barner-Kowollik C. Macromolecules. 2012; 45:5012.
90. Kennedy DC, McKay CS, Legault MCB, Danielson DC, Blake JA, Pegoraro AF, Stolow A, Mester Z, Pezacki JP. J Am Chem Soc. 2011; 133:17993. [PubMed: 21970470]
91. Haldón E, Nicasio MC, Pérez PJ. Org Biomol Chem. 2015; 13:9528. [PubMed: 26284434]
92. Yang M, Jalloh AS, Wei W, Zhao J, Wu P, Chen PR. Nat Commun. 2014; 5:4981. [PubMed: 25236616]
93. Agard NJ, Prescher JA, Bertozzi CR. J Am Chem Soc. 2004; 126:15046. [PubMed: 15547999]
94. Dommerholt J, van Rooijen O, Borrmann A, Guerra CF, Bickelhaupt FM, van Delft FL. Nat Commun. 2014; 5:5378. [PubMed: 25382411]
95. Gold B, Dudley GB, Alabugin IV. J Am Chem Soc. 2013; 135:1558. [PubMed: 23272641]
96. Poloukhtine A, Popik VV. J Phys Chem A. 2006; 110:1749. [PubMed: 16451004]
97. Poloukhtine AA, Mbua NE, Wolfert MA, Boons GJ, Popik VV. J Am Chem Soc. 2009; 131:15769. [PubMed: 19860481]

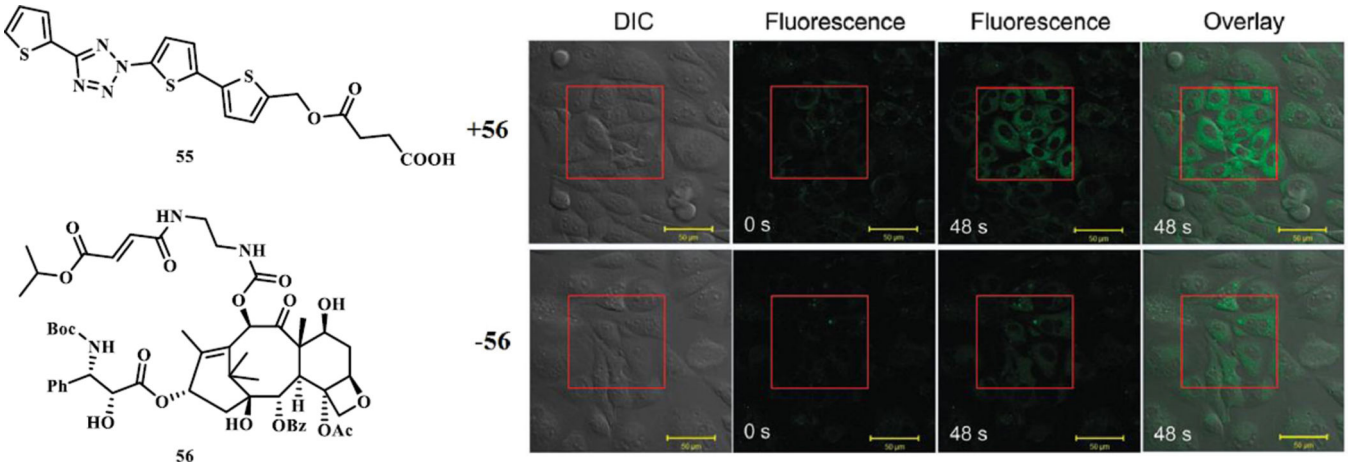


**Fig. 1.**

Fluorescent imaging of microtubules in CHO cells using 405 nm photoactivatable tetrazole **55** in the presence or in the absence of a fumarate-modified docetaxel **56**. The *rectangle area* were illuminated with the 405-nm laser for the indicated time

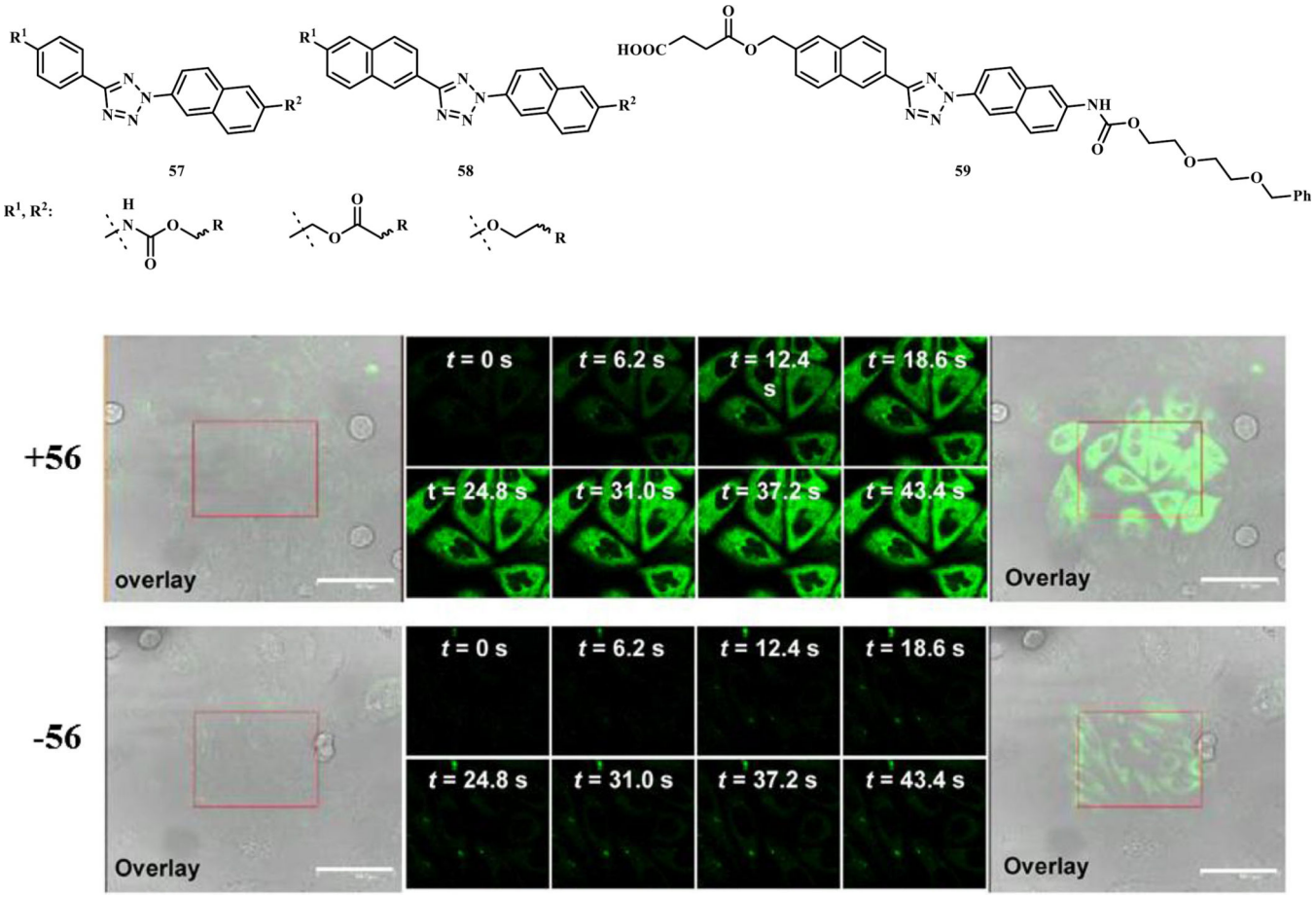


**Fig. 2.**

Structure of 2PE photoactivatable tetrazoles (*top*) and fluorescent imaging of microtubules in CHO cells (*bottom*) using tetrazole **59** in the presence or in the absence of a fumarate-modified docetaxel **56**. The *rectangle area* were illuminated with the 700-nm femtosecond pulsed laser for the indicated time

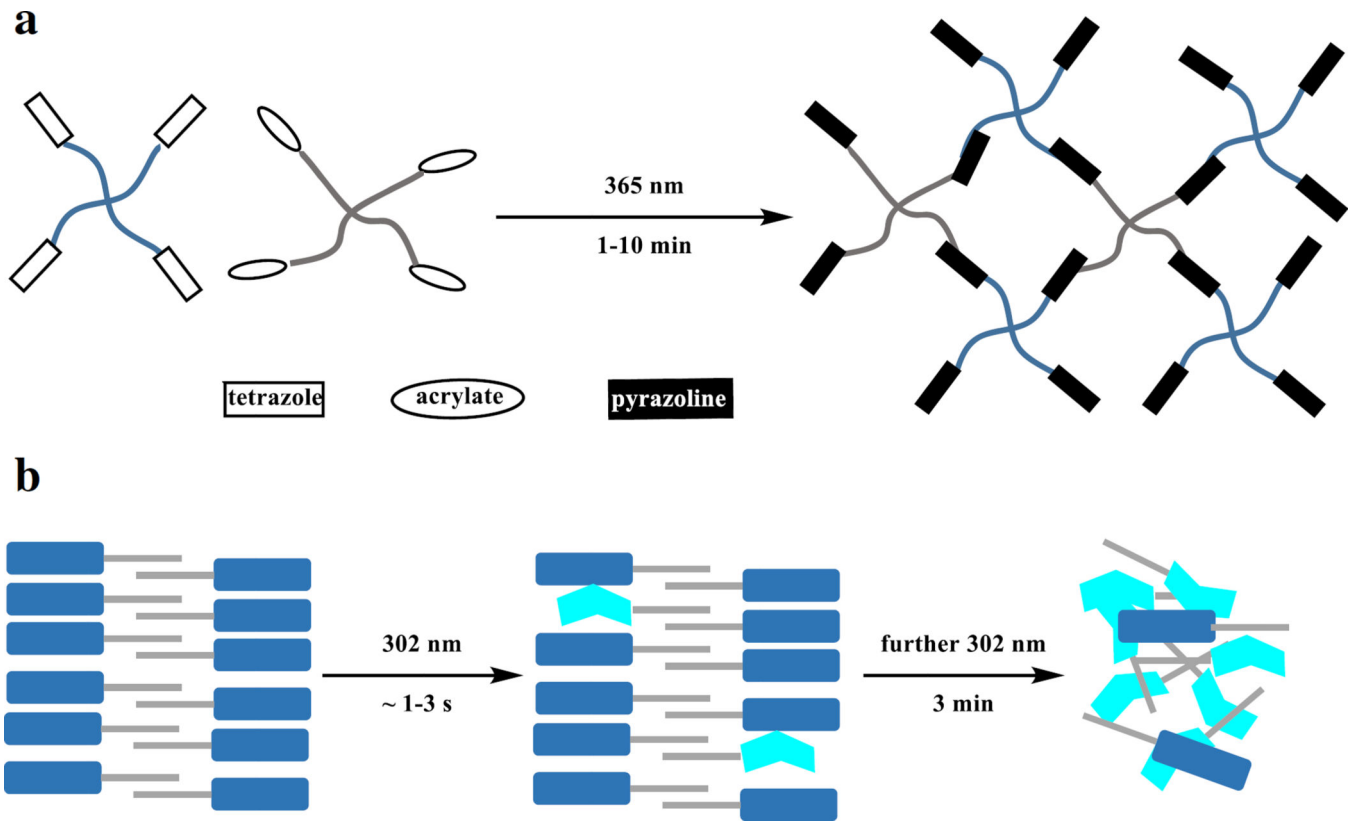


**Fig. 3.**

**a** Hydrogel formation with the tetrazole-based photoclick reaction. **b** The collapse of hydrogels induced by intramolecular photoclick reaction

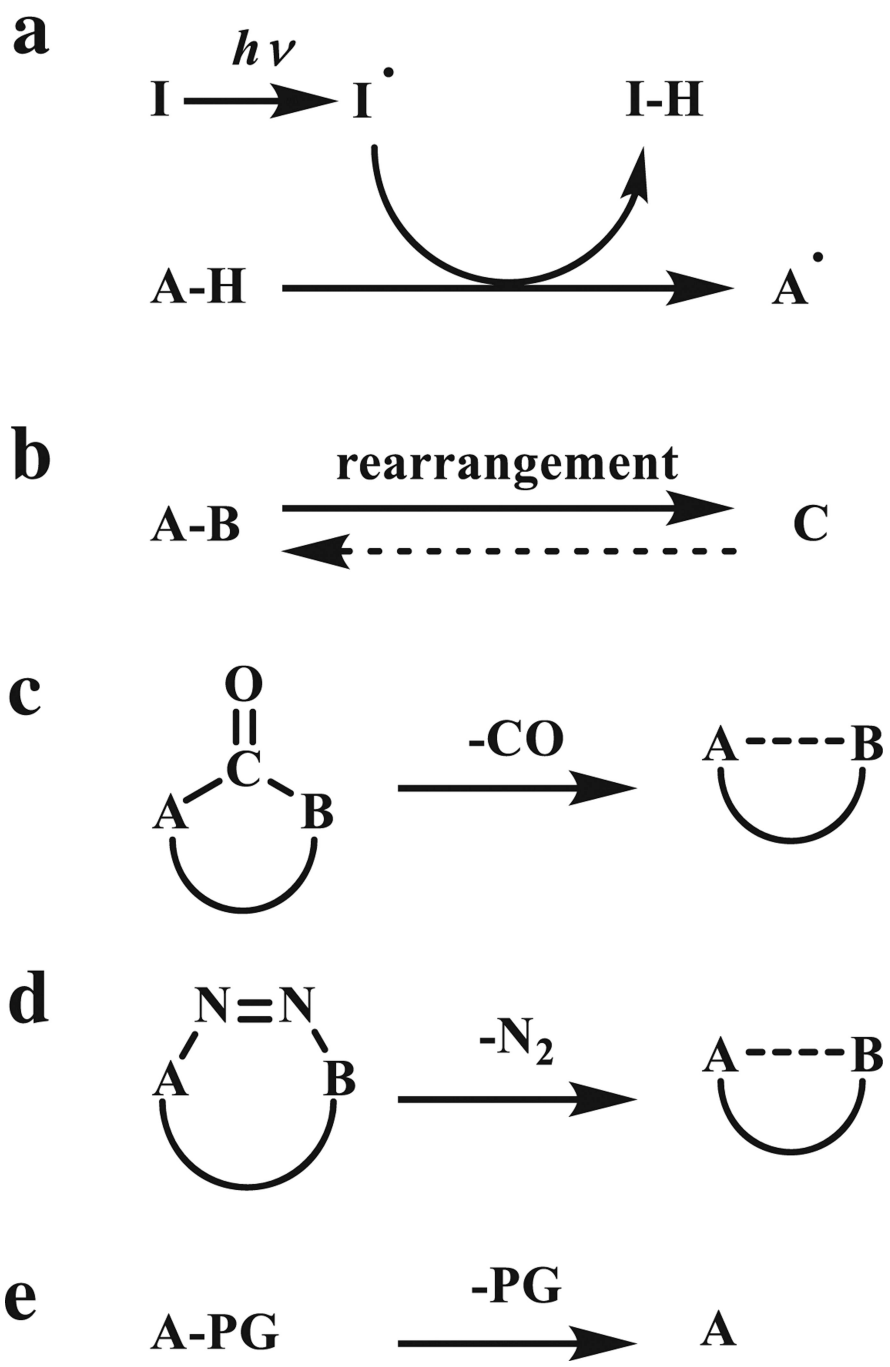


**Scheme 1.**
Photo-triggered generation of reactive intermediates

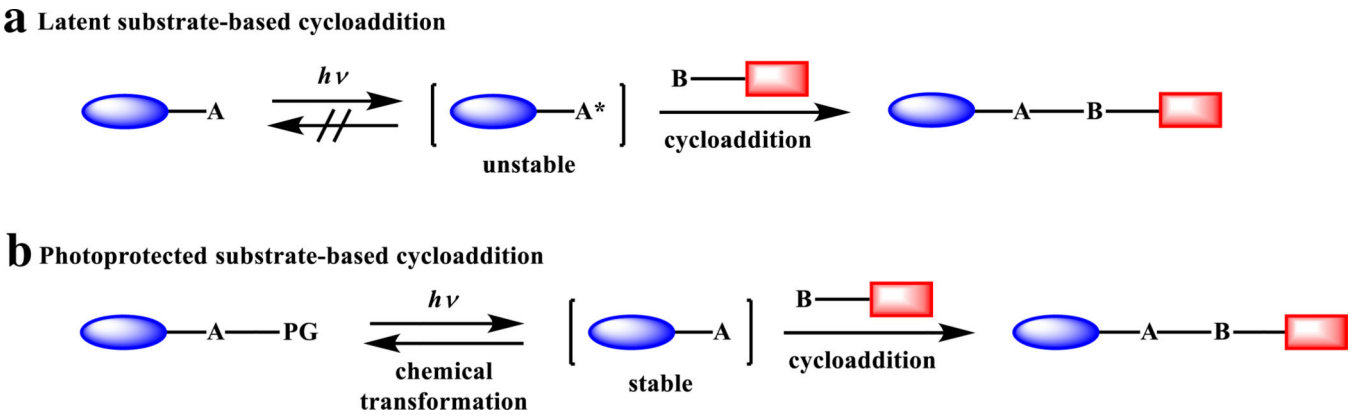


**Scheme 2.**

**a** Strategy based on photoactivation of the precursor to generate a highly reactive and unstable species. **b** Strategy based the removal of a photo-protecting group

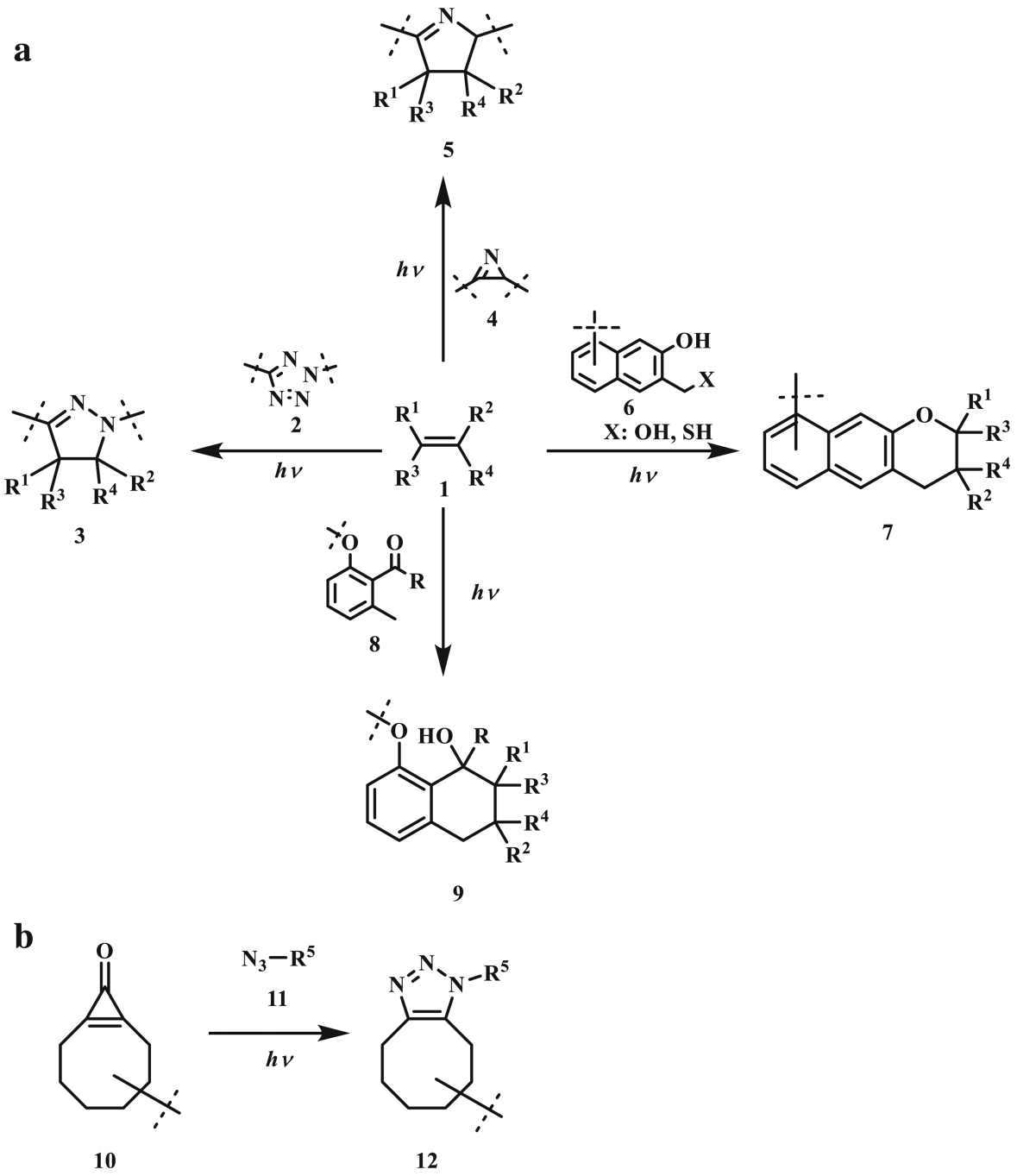


**Scheme 3.**

Summary of photo-triggered cycloaddition reactions useful in biological applications. **a** Reactions between alkenes and photochemically generated 1,3-dipoles or 1,3-dienes. **b** SPAAC between photoprotected cyclooctynes and azides

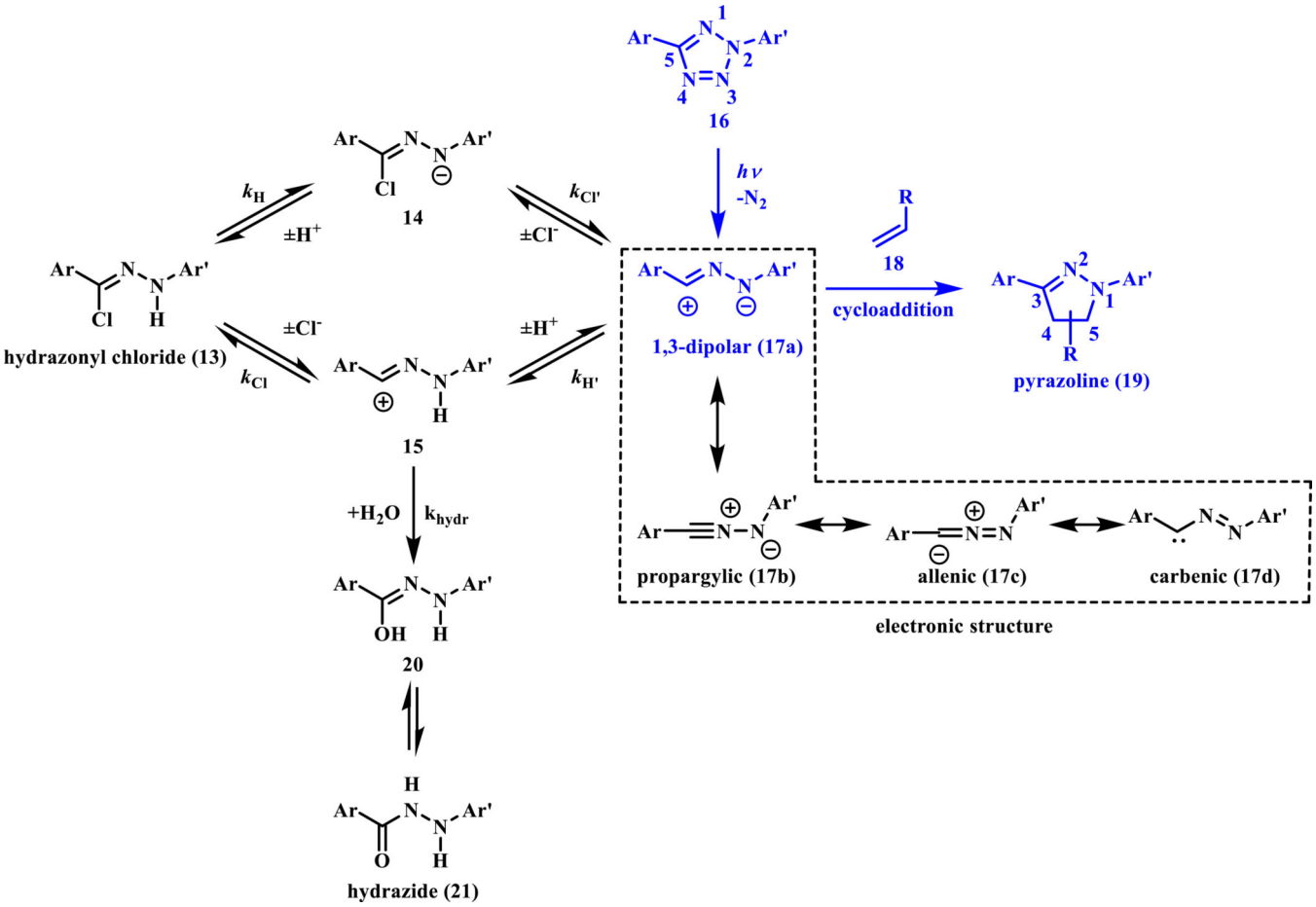


**Scheme 4.**

Plausible mechanistic pathways for the generation of nitrile imine and its reactions in the chloride-containing aqueous medium. The photoinduced tetrazole ring rupture followed by cycloaddition with alkenes are colored in *blue*

**a Reaction of phenylsulfonylhydrazones and arene diazonium salts**

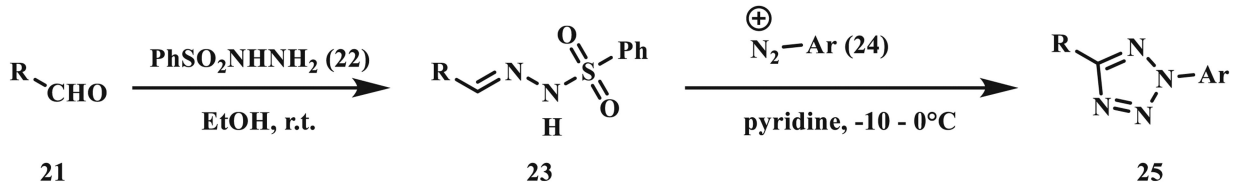


R: alkyl or aryl

**b Thiophene introduction with iodonium salts**

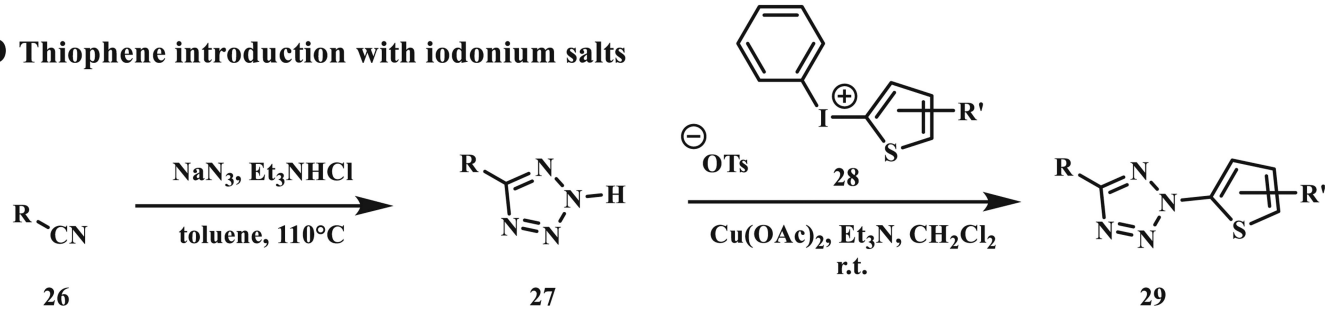


R: alkyl or aryl

**Scheme 5.**
Synthesis of *N*-aryltetrazoles

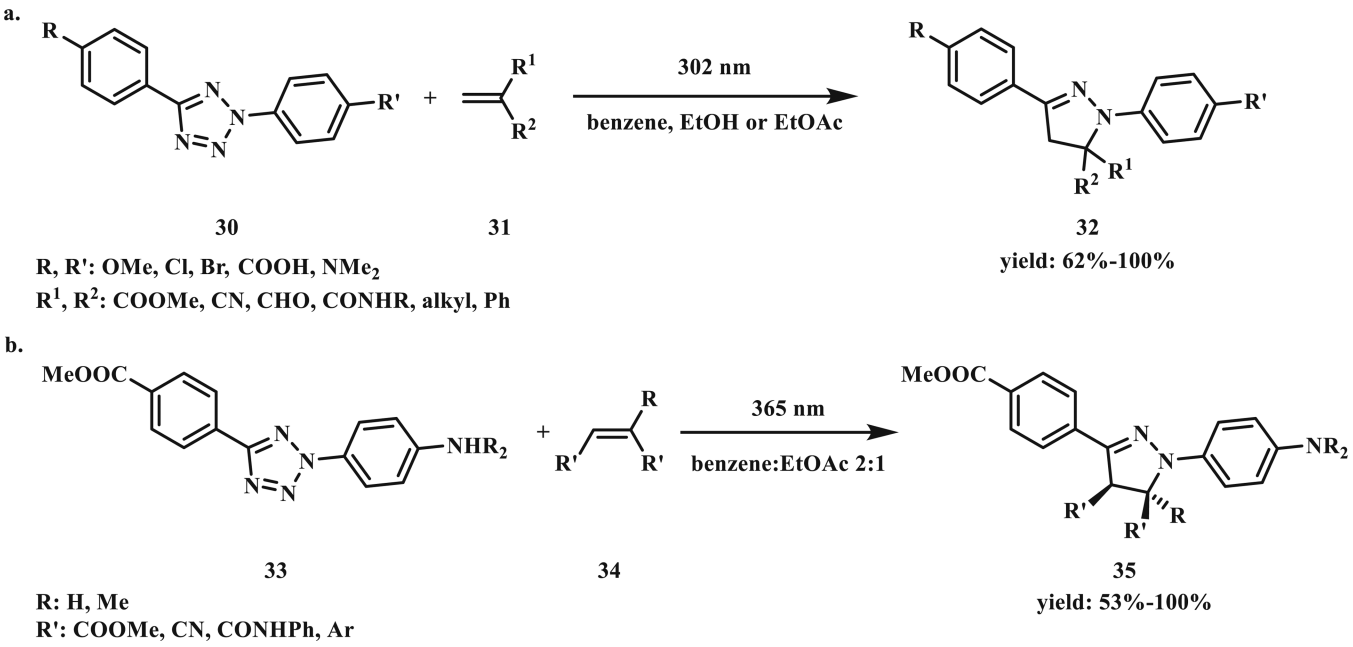


**Scheme 6.**

Reaction of biaryltetrazoles with various dipolarophiles in the photoinduced cycloaddition reaction: **a** first study, **b** optimizing the photoactivation wavelength

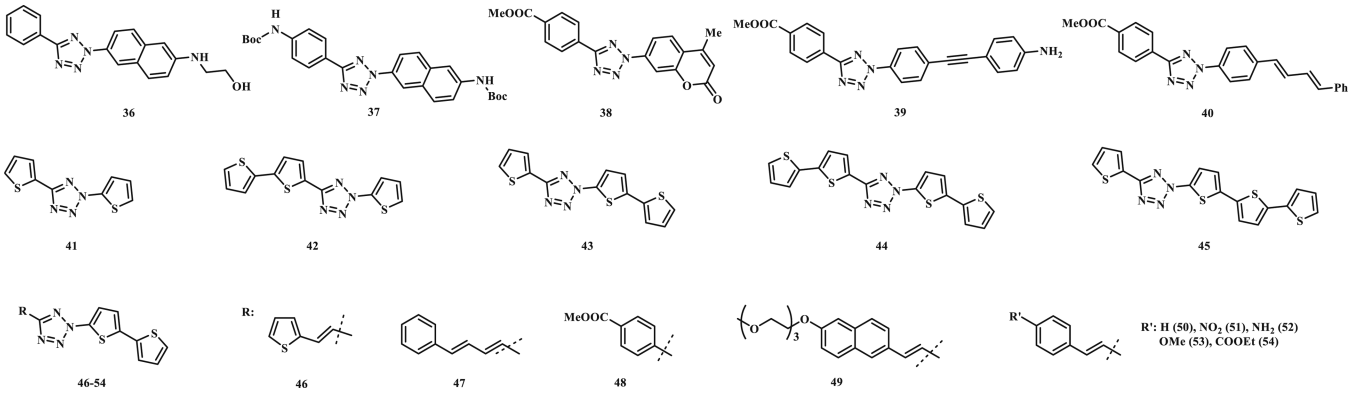


**Scheme 7.**
Tetrazoles with the extended π-systems

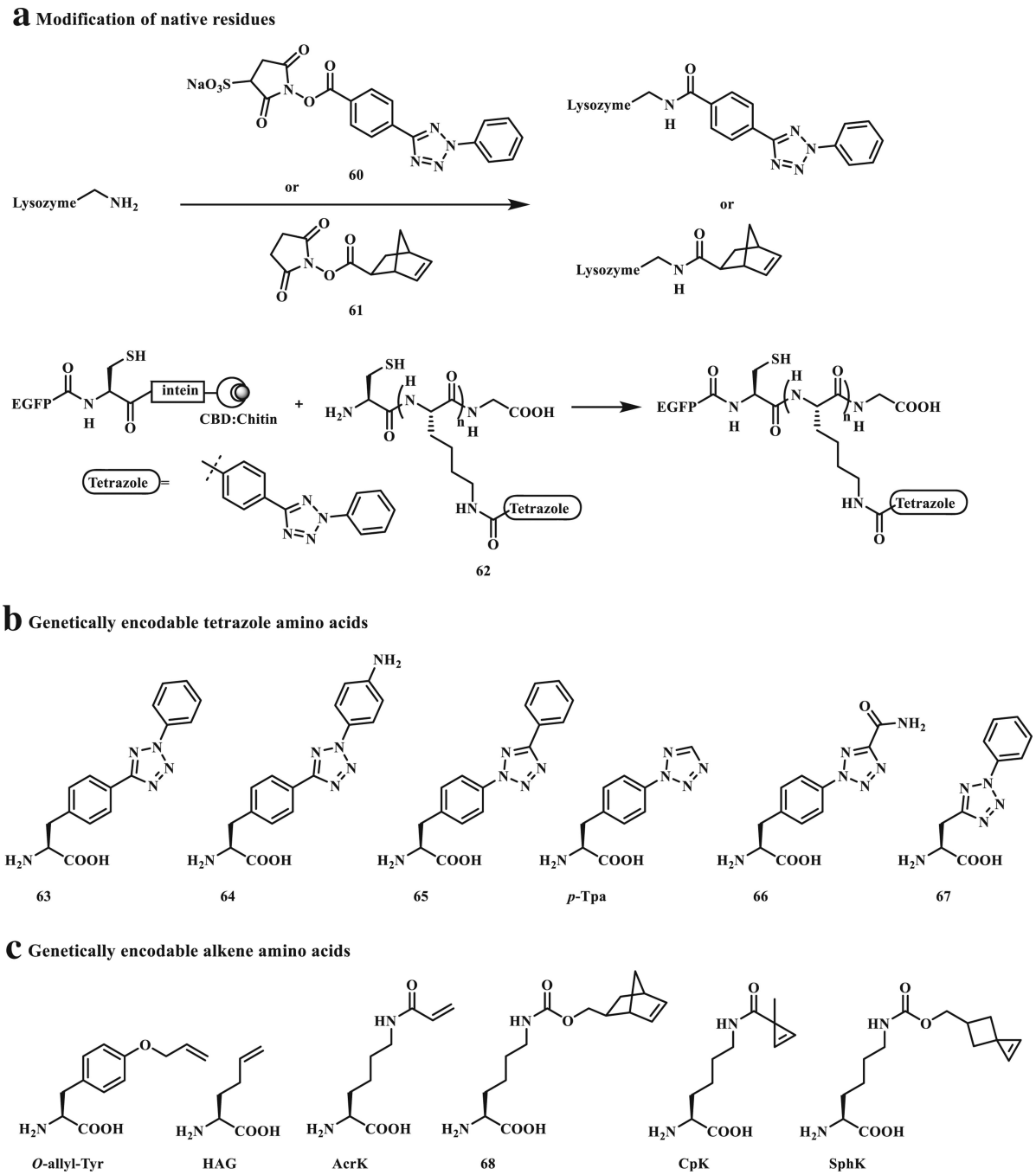


**Scheme 8.**

Strategies for site selective protein modifications via photo-triggered tetrazole-alkene cycloaddition reaction: **a** modification of native residues, **b** genetic encoding of tetrazole amino acids, and **c** genetic encoding of alkene amino acids

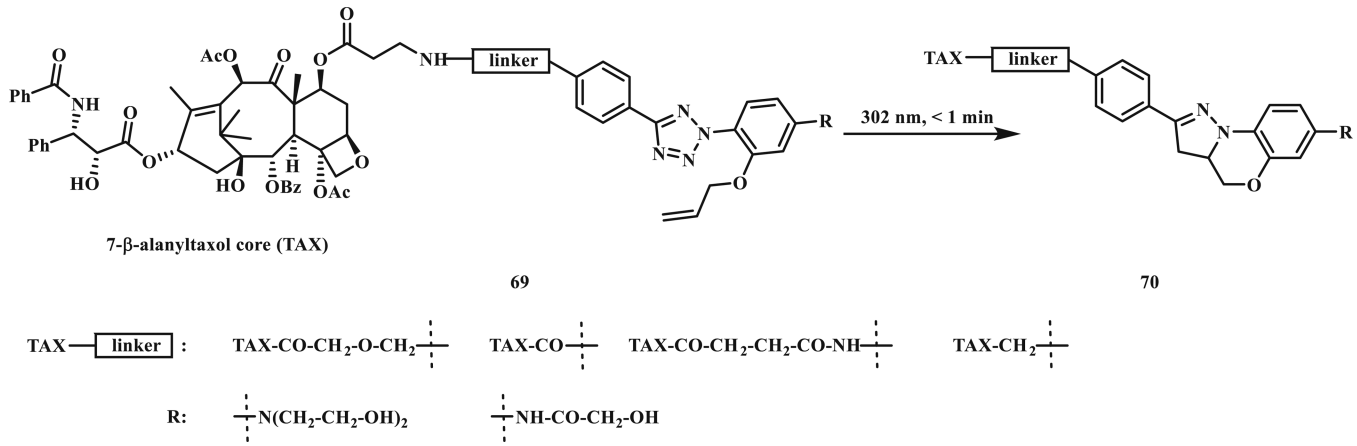


**Scheme 9.**

Tetrazole-based turn-on fluorescent probes for imaging microtubules in live cells

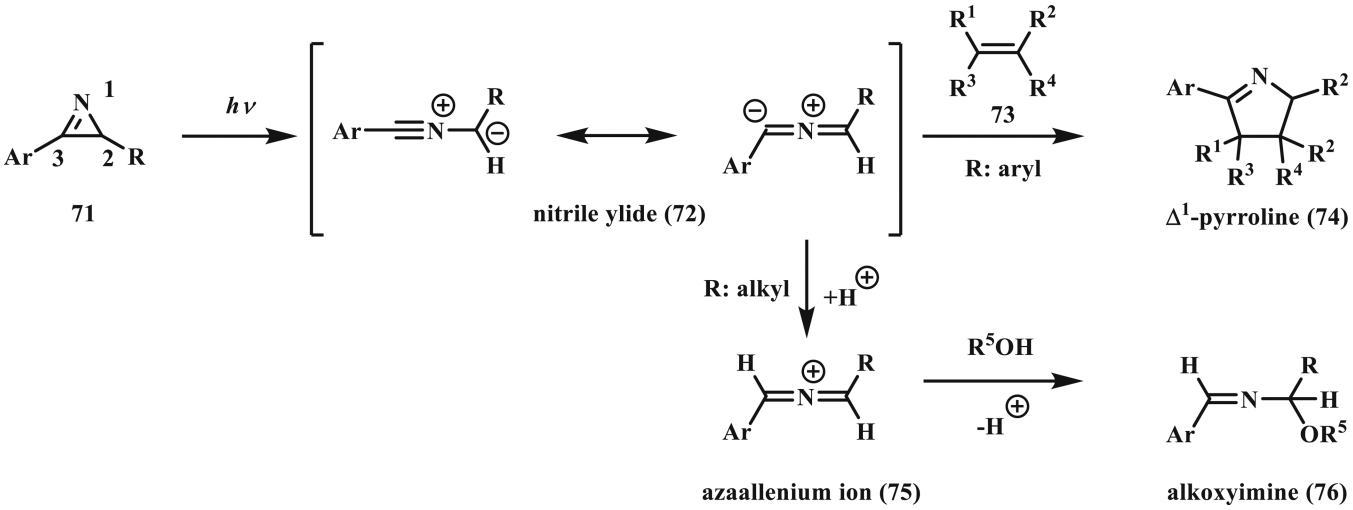


**Scheme 10.**

Photo-triggered reactions of azirines and alkenes or alcohols

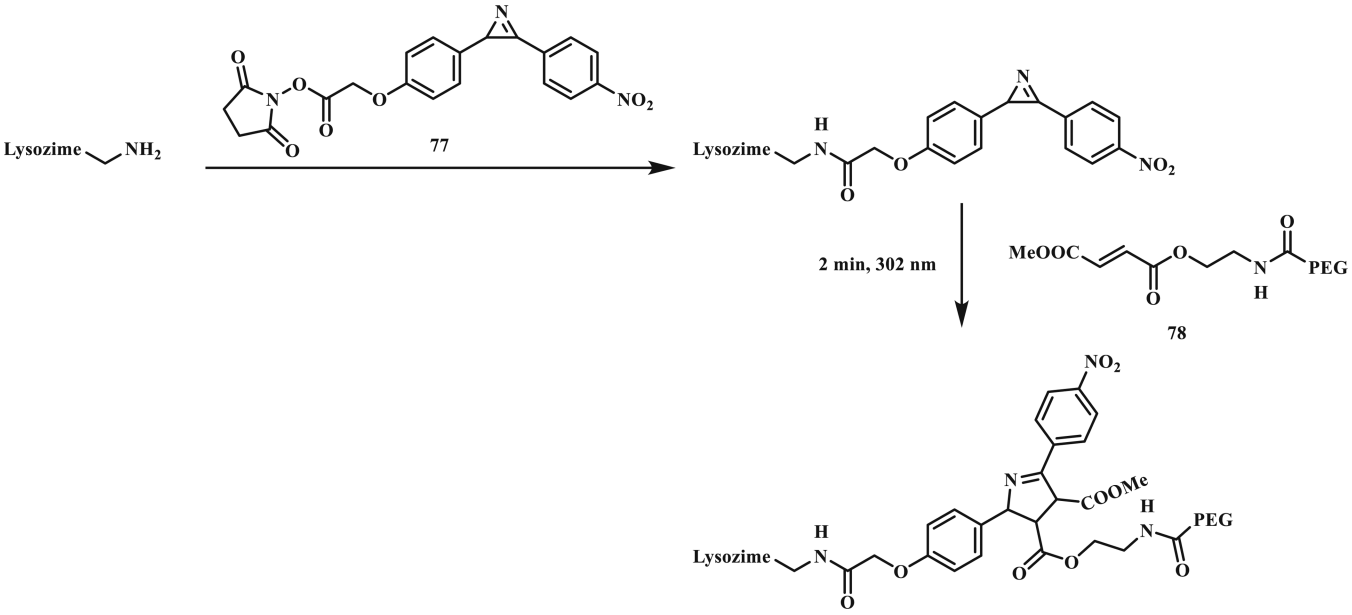


**Scheme 11.**

Selective modification of an azirine-containing lysozyme by a PEG-modified fumarate via a photo-triggered cycloaddition reaction

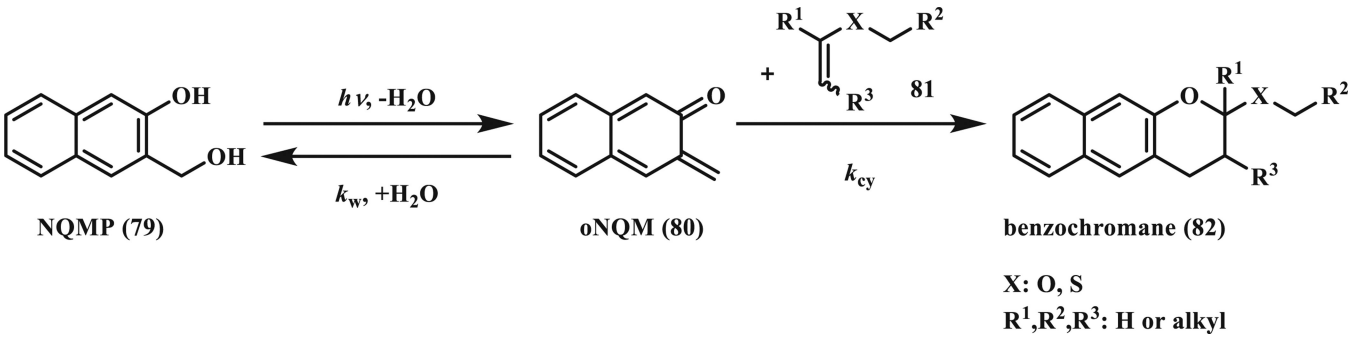


**Scheme 12.**

Photoactivation of NQMP to generate *o*NQM, which then reacts with vinyl (thio)ether

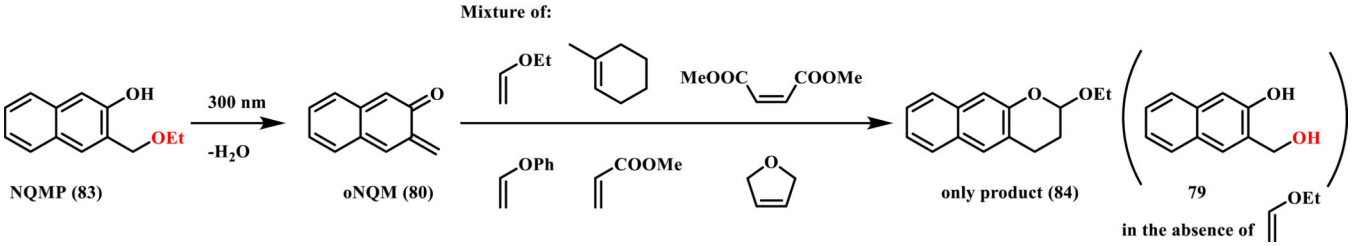


**Scheme 13.**

Substrate scope of the alkene dienophiles in the photo-triggered cycloaddition reaction; product was formed only with ethyl vinyl ether

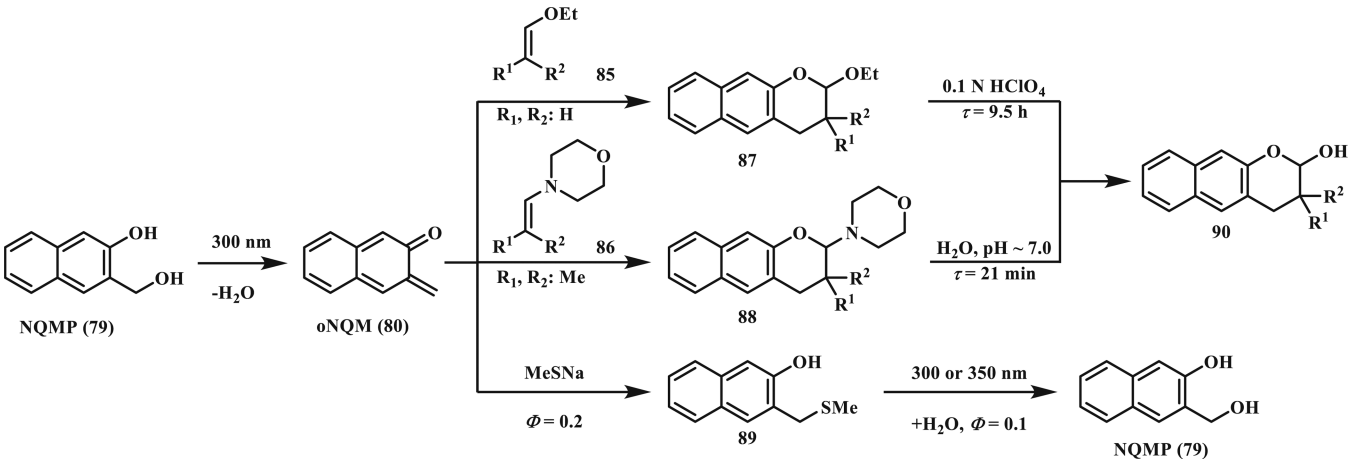


**Scheme 14.**
Reactions between NQM and the electron-rich alkenes or thiol

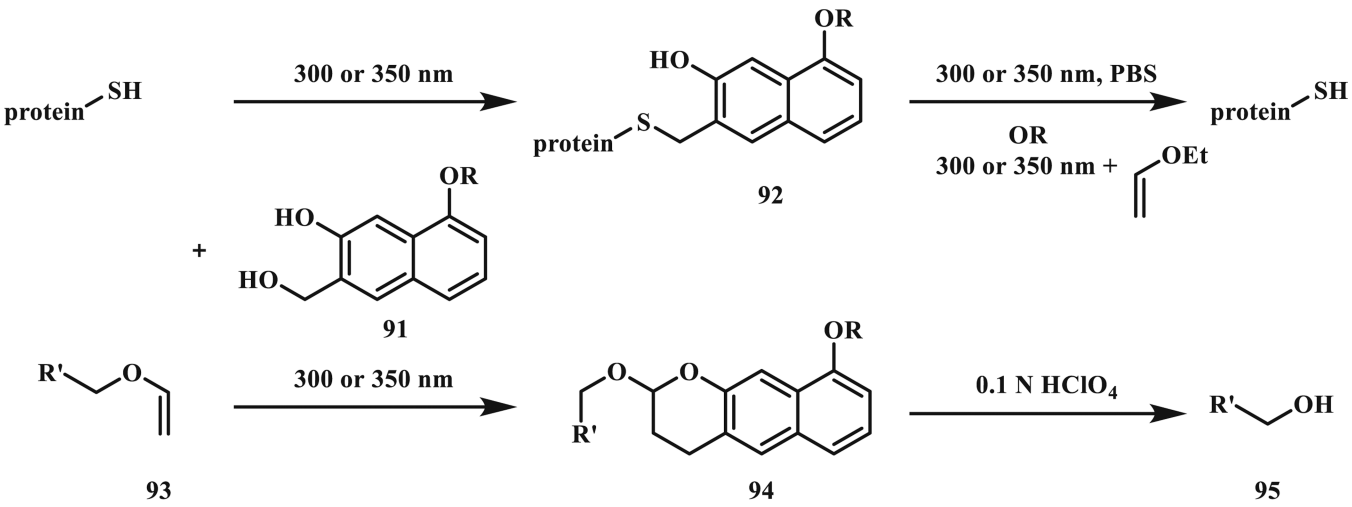


**Scheme 15.**

Exploiting the reversibility: capture with *o*NMQs and release through photolysis or hydrolysis

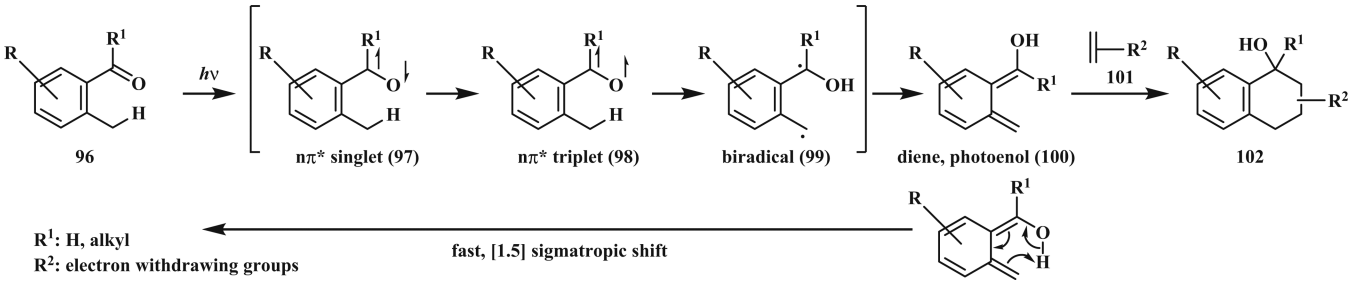


**Scheme 16.**

Mechanism of the photo-triggered isomerization and hetero Diels–Alder reaction of *o*-methyl phenyl ketones and aldehydes

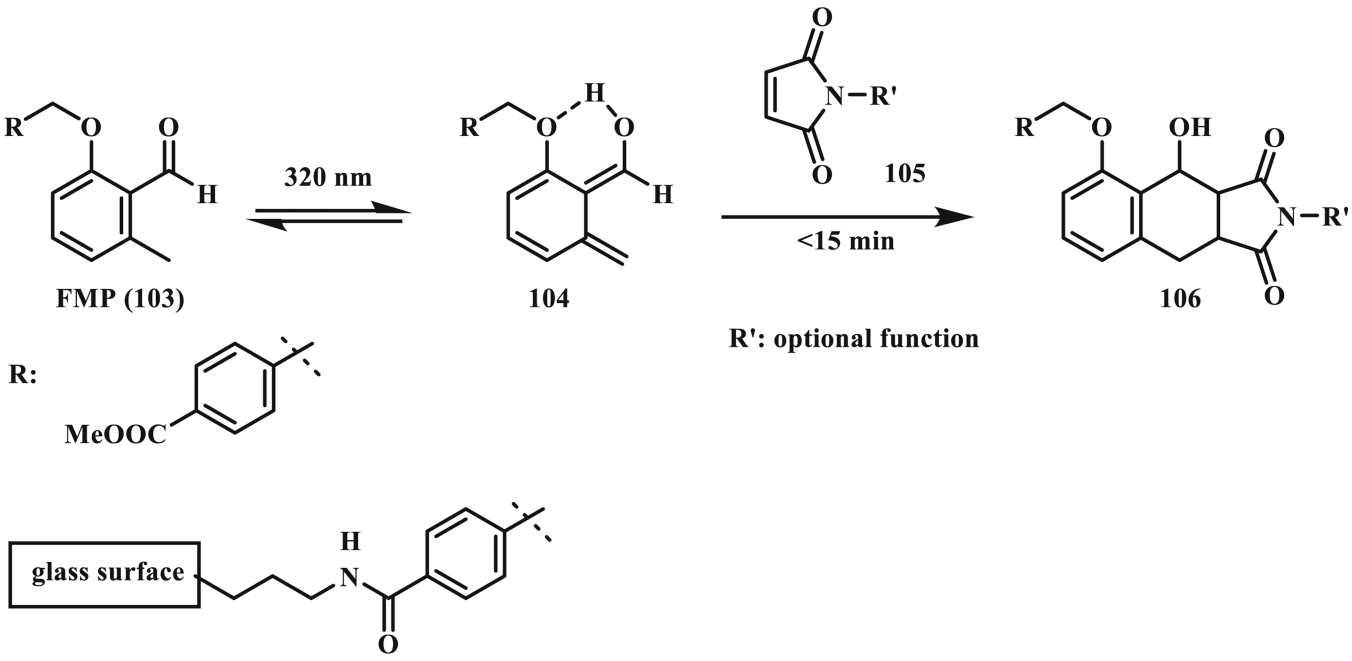


**Scheme 17.**
Photo-triggered hetero Diels–Alder reaction with FMP

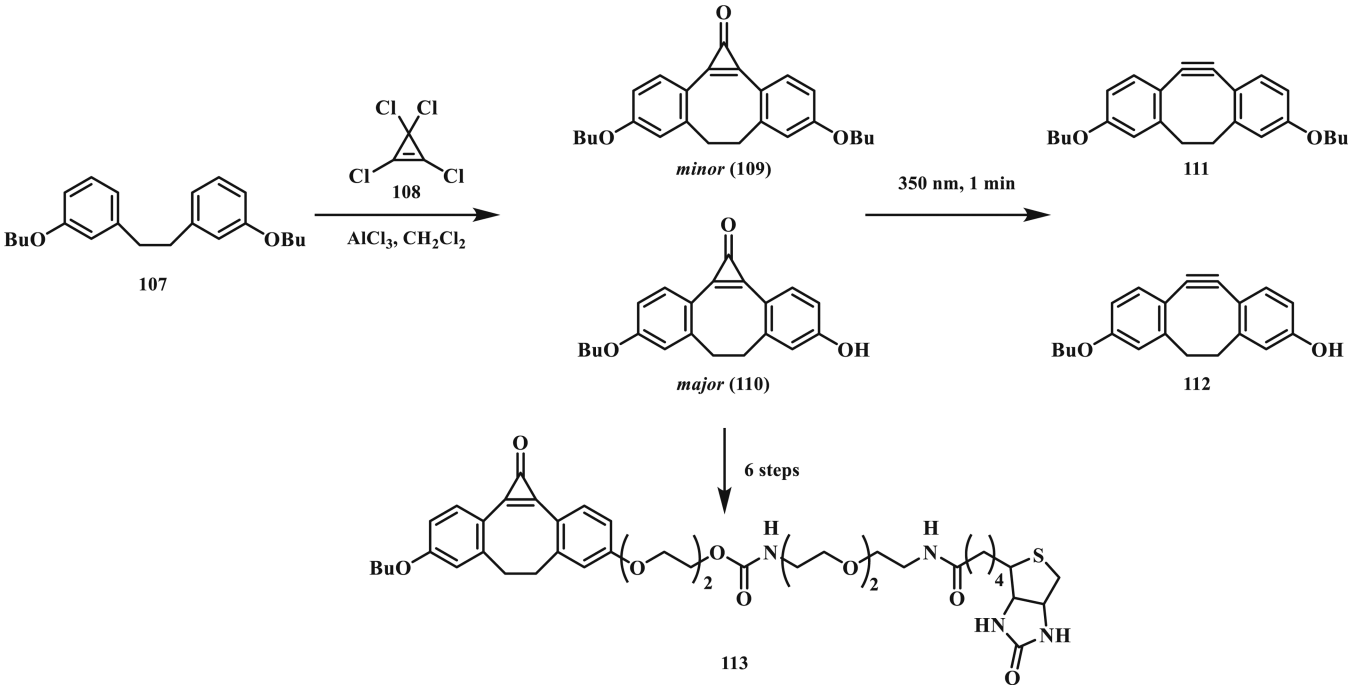


**Scheme 18.**
Synthesis and photodecarbonylation of dibenzocyclopropenones.

**Table 1**

Optimized parameters for the photo-triggered click reactions

| Cycloaddition reaction | Irradiation wavelength | Irradiation time | Rate constant ($k_2$) (solvent) |
|---|---|---|---|
| Tetrazole–alkene | 405, 700 nm (2PE) | ~ 1 min | $3.4 \times 10^4$ $M^{-1}$ $s^{-1}$ (1:1 PB/MeCN) |
| Azirine–alkene | 302 nm | 2 min | 0.0379 $M^{-1}$ $s^{-1}$ (1:1 PBS/MeCN) |
| 3-Hydroxy-2-naphthalenemethanol-vinyl ether | 300, 350 nm | 3–20 min | $4–6 \times 10^4$ $M^{-1}$ $s^{-1}$ (1:1 PB:MeCN) |
| *o*-Methyl phenyl ketone/aldehyde-alkene | 320 nm | 2 h | Not determined |
| Cyclopropenone-azide | 350 nm | 1 min | $7.6 \times 10^{-2}$ $M^{-1}$ $s^{-1}$ (MeOH) |